Atmos. Chem. Phys. Discuss., 12, 10535–10621, 2012
www.atmos-chem-phys-discuss.net/12/10535/2012/
doi:10.5194/acpd-12-10535-2012

Atmospheric Chemistry and Physics Discussions

The changing radiative forcing of fires: global model estimates for past, present and future

D. S. Ward[1], **S. Kloster**[2], **N. M. Mahowald**[1], **B. M. Rogers**[3], **J. T. Randerson**[3], **and P. G. Hess**[4]

[1]Earth and Atmospheric Science, Cornell University, Ithaca, New York, USA
[2]Land in the Earth System, Max Planck Institute for Meteorology, Hamburg, Germany
[3]Earth System Science, University of California, Irvine, California, USA
[4]Biological and Environmental Engineering, Cornell University, Ithaca, New York, USA

Received: 22 March 2012 – Accepted: 11 April 2012 – Published: 24 April 2012

Correspondence to: D. S. Ward (dsw25@cornell.edu)

Published by Copernicus Publications on behalf of the European Geosciences Union.

Abstract

Fires are a global phenomenon that impact climate and biogeochemical cycles, and mediate numerous interactions between the biosphere, atmosphere and cryosphere. These impacts occur on a range of temporal and spatial scales and are difficult to quantify on a global scale based solely on observations. Here we assess the role of fires in the climate system using model estimates of radiative forcing (RF) from global fires in the preindustrial, present day, and future time periods. Fire emissions of trace gases and aerosols were derived from transient simulations with the Community Land Model and then used in a series of Community Atmosphere Model simulations with representative emissions from the years 1850, 2000, and 2100. Additional simulations were carried out with fire emissions from the Global Fire Emission Database for a present-day comparison. Reduced land carbon storage due to fires suggests a large preindustrial positive RF from atmospheric CO_2. This effect of fires also limits the amount of carbon that can be released during the large-scale conversion of forests to agricultural land that took place during the 19th and 20th centuries, resulting in a negative change in RF from fire-emitted CO_2 from the year 1850 to 2000. The remaining greenhouse gas forcings from fire emissions (methane, nitrous oxide and ozone) were smaller in magnitude. The indirect radiative effects of fire aerosols on clouds are dominant in the present and future time periods with a negative RF (cooling) of $1.0\,W\,m^{-2}$ or greater for all time periods. We also consider the impacts of fire on the aerosol direct effect, land and snow surface albedo, and indirect aerosol effects on biogeochemistry, which lead to small RFs. Overall, we conclude that fires are responsible for an RF of about $-1.2\,W\,m^{-2}$ in the preindustrial climate (with respect to a preindustrial climate without fires), and human activities have increased the RF of fires by about $0.7\,W\,m^{-2}$ from 1850 to 2000 and potentially $0.4\,W\,m^{-2}$ from 1850 to 2100 in the model representation by a combination of effects on fire activity and on the background environment in which fires occur. Thus, fires play an important role in both the natural equilibrium cli-

ACPD

12, 10535–10621, 2012

mate and the climate perturbed by anthropogenic activity and need to be considered in future climate projections.

1 Introduction

Fires impose a considerable forcing on the global climate through impacts on a diverse set of Earth system processes (Bowman et al., 2009). These include land and ice surface energy budgets, biogeochemical cycling, and physical and chemical processes in the atmosphere. Recent studies have begun to quantify various aspects of fires' effects on climate. These studies have focused on specific impacts (e.g., Liu et al., 2005; Naik et al., 2007; Ito et al., 2007), certain types of fire emissions (e.g., Jacobson, 2004), or on fires that occur within a particular ecosystem or region (e.g., Randerson et al., 2006; Pfister et al., 2008; Stone et al., 2011). More general assessments highlight the complexity of these impacts, particularly those from aerosols, and the difficulty in performing a comprehensive analysis at a global scale (Forster et al., 2007; Bowman et al., 2009). As such, the sum radiative effect of fires on a global scale remains fundamentally uncertain (Carslaw et al., 2010).

When an open fire burns, products of the combustion are released into the atmosphere both as aerosols and trace gases, including important greenhouse gases (Fig. 1). Global emissions of carbon dioxide (CO_2) due to fires were estimated to be 2.0 Pg carbon(C) yr^{-1} averaged from 1997 to 2009 by van der Werf et al. (2010), of which approximately 0.5 PgC yr^{-1} is associated with deforestation, contributing to the net buildup of CO_2 in the atmosphere. Fire emissions also contain other key greenhouse gases, including methane (CH_4) and nitrous oxide (N_2O) (Andreae and Merlet, 2001). Moreover, the flux of high concentrations of carbon monoxide (CO), other nonmethane hydrocarbons (NMHCs), and NO_x ($NO + NO_2$) alters the oxidation capacity of the atmosphere, potentially leading to a modified CH_4 lifetime and locally high concentrations of the short-lived greenhouse gas, ozone (O_3). Fire-produced O_3 has been

ACPD
12, 10535–10621, 2012

shown to impact the radiation budget on a global scale over the anthropocene (Ito et al., 2007).

According to estimates compiled by Andreae and Rosenfeld (2008) for the year 2000, fires are the largest source of primary carbonaceous aerosol mass globally. Aerosol emissions from fires consist mainly of organic carbon (Galanter et al., 2000; Andreae and Merlet, 2001) but also contribute to global black carbon emissions (Schwarz et al., 2008; Mieville et al., 2010). Together, these particles scatter and absorb radiation, exerting a direct aerosol effect on the radiation budget. However, estimates of the global direct effect due to present-day fires disagree on the sign of the forcing (Forster et al., 2007). In addition, aerosols alter climate by their impacts on clouds. Some aerosol species, especially black carbon, add heat to the cloud environment leading to evaporation, which alters the radiative balance (the semi-direct effect), and aerosols act as cloud condensation nuclei and ice nuclei to modify the cloud albedo and lifetime (Lohmann and Feichter, 2005). After returning to the land surface, either by dry or wet deposition, fire aerosols can apply further forcing onto the climate by transporting nutrients or toxins to sensitive ecosystems (Chen et al., 2010; Mahowald, 2011). Also, black carbon deposition on snow and ice surfaces has been shown to reduce the surface albedo in the visible spectrum (Hadley et al., 2010) contributing to changes in the global radiation budget (Flanner et al., 2007, 2009).

In the immediate aftermath of a fire, the albedo of the burned area is typically reduced as the surface may be charred. But over longer time periods, an opening of the canopy can expose higher albedo surfaces such as grass and shrub vegetation, or snow, leading to a negative radiative forcing in some ecosystems (Randerson et al., 2006). Regrowth of vegetation following a fire sequesters CO_2 from the atmosphere, compensating for the emission of CO_2 during the fire. However, the magnitude of the C sink may be quite different than the magnitude of the original C source, especially in a case such as deforestation fires in which agricultural land often replaces the forest (Jacobson, 2004). Over a period of years to decades, post-fire changes in the age and

ACPD
12, 10535–10621, 2012

composition of vegetation can alter the surface energy budget (Liu et al., 2005) and the local biogeochemical cycling (Thonicke et al., 2001; Thornton et al., 2007).

Fires occur naturally and have for many millions of years prior to human influences (Bowman et al., 2009). In recent times however, human activity has played a large role in both igniting and suppressing fires, as well as modifying fire regimes through land-use change (Marlon et al., 2008). Fires are likely to respond to future climate changes since fire activity depends on long-term precipitation, temperature, and humidity trends (Kloster et al., 2012). Recent development of global fire prediction schemes (Thonicke et al., 2001, 2010; Arora and Boer, 2005; Kloster et al., 2010; Prentice et al., 2011) has made it possible to simulate the spatial distribution of past (pre-satellite era) and future fire emissions within a global land model.

In this study we assess fire impacts on climate using estimates of fire emissions from the Kloster et al. (2010) scheme implemented in the Community Land Model (CLM) and from the Global Fire Emissions Database (GFED) (van der Werf et al., 2010). We use the concept of radiative forcing (RF) as a measure of climate impacts with an aim toward evaluating the relative importance of each of the various fire/climate forcings. We estimate the global RF of fires for 1850, 2000, and 2100 by their impacts on long-lived greenhouse gases (CO_2, CH_4, N_2O), O_3, the aerosol direct effect, aerosol indirect effects, aerosol deposition on snow/ice surfaces, surface albedo changes and changes to biogeochemical cycles (Fig. 1) using a modeling approach described in the following section.

2 Methods

The RF of the various fire impacts shown in Fig. 1 are isolated by comparing the atmosphere and land simulated with fire effects (emissions, ecosystem disturbance), to the same atmosphere and land but simulated without fire effects. The differences between the "fire" and "no-fire" model output were considered to be representative of the impacts of fires. This approach is fundamentally different from efforts to estimate fire RFs from

ACPD
12, 10535–10621, 2012

a single set of simulations that include both fire emissions and all other emissions. The major distinction is that in our "no-fire" world, in the absence of fire emissions, non-fire trace gases and aerosols will evolve differently than in the "fire" world simulation that includes all emissions.

Comparing a fire world to a no-fire world required several simplifications that we note here. The land and ice surface albedos remain constant between fire and no-fire simulations, although in a no-fire world albedo fields could be quite different. Similarly, CO_2 concentrations, which are impacted by removing fires, are kept identical in the fire and no-fire simulations. Fires also emit nitrogen (N)-containing species and effect N deposition, but this impact is not removed when we exclude fire emissions from our simulations, which use standard N-deposition input datasets. These assumptions greatly reduce the complexity of the model experimental setup. In addition, the model configuration used for this study does not include dynamic vegetation (needed to simulate succession), or aerosol effects on convective cloud droplet number.

To address some of the uncertainty in the model fire emissions datasets, results for present-day RF from the CLM fire emissions are compared to the estimates from the GFED emissions for the same time period. All atmosphere simulations use a climate representative of the year 2000, and we assume that future land-use changes follow Representative Concentration Pathway (RCP) 4.5 and future greenhouse gas concentrations follow SRES A1B (Nakicenovic et al., 2000), which is similar to the RCP 4.5 greenhouse gas concentration trajectory (Moss et al., 2010).

2.1 Fire emissions

Global fire emissions were derived from simulations documented by Kloster et al. (2010, 2012) using a modified form of the Community Land Model CLM3 (Oleson et al., 2008a; Stockli et al., 2008). Emissions from fires are predicted in CLM3 with the coupled carbon-fire model implemented by Kloster et al. (2010) building on work from Arora and Boer (2005). The model combines fuel availability, fuel moisture content and ignition probabilities with the model wind to explicitly predict the area burned. Kloster

ACPD
12, 10535–10621, 2012

et al. (2010) introduced an anthropogenic impact on fire ignition and suppression based on population. Emissions from deforestation fires are represented as a fraction of the C lost due to land-use change.

CLM version 3.5, hereafter CLM3, includes modifications to the hydrology scheme, improved representation of soil properties, treatment of urban land cover, and improvements to the snow pack dynamics (Decker and Zeng, 2009; Sakaguchi and Zeng, 2009; Niu and Yang, 2007; Flanner and Zender, 2005; Flanner et al., 2007; Wang and Zeng, 2009; Lawrence and Slater, 2008, 2009; Oleson et al., 2008b). Additionally, these simulations used the carbon-nitrogen biogeochemical cycling extension of CLM3 (CN) (Thornton et al., 2007, 2009). The CN model tracks storage and fluxes of carbon and nitrogen between vegetation, soil, and litter pools, and introduces nitrogen limitation on primary production.

CLM3 was run as described above with 1.9° latitude by 2.5° longitude grid spacing for the years 1798–2100 (Kloster et al., 2010, 2012). Atmospheric forcing from the Qian et al. (2006) NCEP/NCAR reanalysis for 1948 to 1972 was repeatedly cycled during the model years 1798 through 1972 with the last 25 yr corresponding exactly to the reanalysis. After 1972 and through to 2100, the same reanalysis dataset was cycled but climate anomalies relative to the 1948 to 1972 period are applied. The anomalies were defined as the difference between monthly mean future projections and the base period (1948–1972) reanalysis. They were derived from three ensemble runs from the coupled climate models ECHAM5/MPI-OM (hereafter ECHAM) (Roeckner et al., 2006) and three from the Community Climate System Model (CCSM) (Meehl et al., 2006) all using the SRES A1B scenario (Nakicenovic, 2000). Transient atmospheric CO_2 concentration was taken from the same scenario. N deposition followed the transient record from Lamarque et al. (2005) through the year 2004 and was kept constant at present day levels through the year 2100.

Transient population density and land cover were also used from 1850 to 2100. Land cover changes for 1850 to 2000 follow Hurtt et al. (2006) and were implemented in CLM as plant functional type (PFT) changes (Lawrence et al., 2011). Future land-use

ACPD
12, 10535–10621, 2012

changes follow the projection from RCP 4.5. All the future RCP scenarios for land-use change cause a decrease in global fire emissions (including deforestation fire emissions) between the year 2000 and the years 2075 to 2099 by reducing the biomass available for burning (Kloster et al., 2012). The RCP 4.5 land-use change leads to the smallest decrease in fire emissions of all the RCPs, 5 %, compared to the maximum decrease of 30 % when RCP 8.5 is used (Kloster et al., 2012). The range in projected fire emissions informs on this aspect of the uncertainty in our future fire emissions estimates.

2.1.1 Carbon loss due to fires

Monthly fire emissions were derived from the CLM3 total C lost due to fire (FIRE_CLOSS) that includes deforestation fires. The amount of C lost in fires gradually increases through the 1950s, but then slightly decreases to 2000 (Fig. 2); projection of future tendency is dependent on the atmospheric forcing, showing a steep increase in carbon lost for the ECHAM forcing and very little trend with the CCSM forcing. For pre-industrial emissions, FIRE_CLOSS was averaged for each month for the period 1845 to 1854 (hereafter named 1850). For present-day emissions we compute the 1997 to 2006 average and for future emissions, 2090–2099 (hereafter named 2000 and 2100, respectively). The 1997 to 2006 average used the ensemble average of the CCSM climate forcings, which was very similar to the ECHAM ensemble average for these years (Kloster et al., 2012). We use decadal means to diminish the impact of the large interannual variability of fire emissions on the single year used to drive the model emissions, as in Lamarque et al. (2010). The two future climate forcing ensembles are averaged separately to create two future datasets, ECHAM and CCSM. In addition, fire emissions estimates from the GFED version 2 (GFEDv2) (van der Werf et al., 2006) were applied as a comparison to the present-day CLM3 derived emissions.

Comparisons of the CLM3 FIRE_CLOSS to that from GFEDv2 suggest that the model underestimates the globally averaged GFEDv2 carbon emissions for the present day period (Fig. 2). This bias results in large part from a disparity in the area burned by

ACPD
12, 10535–10621, 2012

Northern Hemisphere tropical fires (Fig. 3a). Furthermore, CLM3 tends to overestimate mid-latitude fire area burned, especially in North America, and does not capture high-latitude fires in the Northern Hemisphere. At the same time, CLM3 underestimates the amount of carbon lost per area burned compared to the GFEDv2 inventory in these regions, as shown in Fig. 3b, indicating a higher proportion of forest to grass (or tundra) burning in GFEDv2. While this disparity appears subtle, it may be important for the RF of fires since aerosol emissions from these high-latitude fires have implications for snow surface and land surface albedo changes (Randerson et al., 2006; Flanner et al., 2007). Elsewhere on the globe, the carbon lost per area burned is similar for all fire emission datasets: this is expected, as during model development the results were compared to GFEDv2 (Kloster et al., 2010).

2.1.2 Application of emission factors

FIRE_CLOSS is converted to emissions of various gas-phase and aerosol species using the emission factors given by Andreae and Merlet (2001) and updates for CO_2, CO, NO_x, SO_2, and organic carbon and black carbon aerosols by Hoelzemann et al. (2004). The Andreae and Merlet (2001) factors were derived for three major biomes (tropical forest, extratropical forest, and savannah and grassland) for which different burning intensities are characteristic, typically dependent on the amount of smoldering. The area burned for each of these biomes is given in Fig. 3c, with savanna and grasslands broken into four categories also containing extra-tropical shrubs and crops. Here we use the CLM3 land cover classification for the GFEDv2 area burned product as well. A larger fraction of the area burned in the GFEDv2 inventory was grassland (particularly tropical grassland) compared to CLM3, which tended to predict more mid-latitude forest area burned than GFEDv2 (Fig. 3a).

A new set of fire emission factors was recently published (Akagi et al., 2011) but was not available for the current fire emissions study. The Akagi et al. (2011) factors include a higher rate of smoldering in boreal forest fires, leading to higher extratropical

ACPD
12, 10535–10621, 2012

forest fire emission factors for CO, CH_4, and primary organic aerosols when compared to Andreae and Merlet (2001).

Emission factors are given as the mass emitted per unit mass of dry matter burned. A carbon content factor is used to convert between the dry matter burned and FIRE_CLOSS predicted by the model. We assume a C content of the burned matter equal to the total mass of the C emitted as CO_2 and CO per unit mass of dry matter as defined in the emission factors. Other C-containing species do not have an appreciable effect on the total C emitted. The resulting biome-dependent C contents are comparable to the constant value of 45 % used by van der Werf et al. (2006).

CLM3 simulates the land surface for 16 PFTs. For the purpose of calculating emissions, these are classified into the three major biomes as defined by Andreae and Merlet (2001). All grass PFTs are considered savanna and grassland, temperate and boreal forest PFTs are considered extratropical forests, and the remaining forest PFTs are aggregated into the tropical forest biome. The fraction of each PFT within a gridpoint is multiplied by the FIRE_CLOSS at that gridpoint to give the amount of C lost from each PFT. The C lost is converted to dry matter using the C content and multiplied by the emission factor to give the mass of 22 different gas and aerosol species. These are CO_2, CO, CH_4, 12 additional non-methane hydrocarbons, SO_2, NH_3, NO, and black carbon and organic carbon aerosol. The aerosol species are split into hydrophobic and hydrophilic categories according to Emmons et al. (2010).

2.1.3 Treatment of N loss from fires

Total N lost due to fires (FIRE_NLOSS) is also predicted by CLM3. We compute the global, annual FIRE_NLOSS as 29 $TgN\,yr^{-1}$, 26 $TgN\,yr^{-1}$, and 37 $TgN\,yr^{-1}$ for 1850, 2000 and 2100 (averaged between the simulations with different atmospheric forcings), respectively. These values are somewhat larger than a recent global estimate from the GFEDv2 of 22.2 $TgN\,yr^{-1}$ (Chen et al., 2010).

The speciation of the lost N also follows the Andreae and Merlet (2001) emission factors, meaning emission of N-containing species is proportional to the C content of

ACPD
12, 10535–10621, 2012

burned matter, or FIRE_CLOSS, not FIRE_NLOSS. Following these emission factors, 25 to 30 % of the emitted N is released as NH_3 or NO_x in all time periods. An additional large fraction is emitted as molecular N (N_2) (Crutzen and Andreae, 1990). Andreae and Merlet (2001) estimate 30 to 40 % of N lost from fires is emitted as N_2, but Chen et al. (2010) find that the value is likely about 50 % with higher percentages in ecosystems with more complete combustion. Adding together contributions from NH_3, NO_x and N_2 using the C-based emission factors, and after small amounts of trace gases N_2O and HCN are considered, there is still a portion of the FIRE_NLOSS, about 20 to 25 %, that is not accounted for in our emissions estimates.

2.1.4 Aerosol emissions

All fire emissions were released into the lowest model level. This follows the recent results of Tosca et al. (2011) and val Martin et al. (2010) that show most fires' emissions remain within the planetary boundary layer in tropical Asia and in North America, respectively. A variable injection height for emissions was found to be a minor factor for predicting the distribution of smoke plumes in the Western United States (Mao et al., 2011), and in Southeast Asia (Zhang et al., 2011). The results of these studies suggest that modifying the injection height is of little importance for assessing the RF of fire aerosols.

Observations of aerosol optical depth (AOD) from the Aerosol Robotic Network (AERONET) have shown that the GFEDv2 inventory underestimates emissions of aerosols from fires in the tropics (Matichuk et al., 2008; Chin et al., 2009; Tosca et al., 2010; Johnston et al., 2012). Koch et al. (2009) note that nearly all models underestimate black carbon (BC) concentrations in biomass burning regions, which they attribute to problems with the emission factors or estimates of the optical properties of smoke. We scaled aerosol emissions from CLM3 and GFEDv2 fires in several regions following the approach of Johnston et al. (2012) to account for this apparent bias. The method and results of the scaling are given in Appendix A.

ACPD
12, 10535–10621, 2012

Other natural and anthropogenic emissions for the three time periods examined in this study were given by the Atmospheric Chemistry and Climate Model Intercomparison Project (ACCMIP) (Lamarque et al., 2010) for the years 1850 and 2000. For the future climate we used the ACCMIP emissions for RCP 4.5, to be consistent with the CLM3 simulations.

2.2 Model experiments

The fire emissions were applied to two sets of atmosphere simulations, one for tropospheric photochemistry and a separate set for aerosols, with an additional group of land model simulations used to assess the RF due to CO_2 emissions (Table 1). We used releases of versions 4 and 5 of the National Center for Atmospheric Research (NCAR) Community Atmosphere Model (CAM) with a data ocean model, i.e. prescribed sea surface temperatures. The climate sensitivity of these CAM releases was analyzed by Gettelman et al. (2012). Separate model versions were required because chemistry was not yet working in the version of CAM with internally mixed aerosols, which allowed us to look at aerosol indirect effects. Model simulations are named by time period, simulation group and by fire emissions with KF denoting CLM3 fires (Kloster et al., 2010, 2012), GF for GFEDv2 fires, CKF for CLM3 fires with CCSM climate, EKF for CLM3 fires with ECHAM climate, and NF for no fires (Table 1).

2.2.1 CHEM simulations

The simulations of tropospheric photochemistry (CHEM) were run with CAM4 using online chemistry from the Model for Ozone and Related chemical Tracers (MOZART), version 4 (Emmons et al., 2010; Lamarque et al., 2011), with a focus on the impacts of fires on ozone and the oxidation capacity of the troposphere. Eight simulations were run with the different fire emissions (including no fire emissions) for two years each, all branched off of a two-year atmosphere spin-up run (Table 1). The final year in each two-year simulation was used for analysis while the first year was considered spin-up

ACPD
12, 10535–10621, 2012

for the atmosphere with the different emissions. Year 2000 climate forcing was used in all eight CHEM simulations. The online chemistry was not interactive with the radiative transfer and, as a result, the model climate was identical in all CHEM simulations.

2.2.2 AERO simulations

Separate simulations that assess the RFs of aerosols (AERO) were run with CAM5, using the three-mode Modal Aerosol Model (MAM3), Liu et al. (2011a). Many aspects of CAM were updated for version 5 (Liu et al., 2011b) including the cloud microphysics, which are relevant here. CAM5 includes the two-moment cloud microphysical scheme for stratiform clouds described by Morrison and Gettelman (2008), which enables prediction of the size of various hydrometeors. With this new scheme, aerosol/cloud interactions and indirect effects can be simulated for stratiform clouds. Other improvements to the cloud microphysics in CAM5 include updates to the ice nucleation and vapor deposition schemes (Gettelman et al., 2010). MAM3 predicts aerosol mass mixing ratios and number mixing ratios for major aerosol species (excluding nitrate aerosols) in three lognormal modes: Aitken, accumulation and coarse. Primary carbonaceous aerosols are emitted directly into internal mixtures with other accumulation mode species. Chemical oxidant distributions were prescribed for the AERO simulations.

Again, year 2000 climate forcing is applied to the AERO simulations, but in this case aerosols were radiatively active. Variations in the aerosol fields feedback onto other atmospheric variables and result in different climate states depending on the initial emissions. To smooth out the differences in the climate state introduced by the aerosols, the model was integrated for six years and the annual average of the final five years of output was used for analysis. Global, annual average surface temperature differences between simulations with and without fire emissions were less than 0.05 °C for all cases, giving us confidence that atmospheric temperature adjustments were a minor impact on the RFs. As with the CHEM simulations, all the AERO runs were branched from a two-year atmosphere spin-up run.

ACPD
12, 10535–10621, 2012

Both versions of CAM in this study use a grid spacing of the finite volume dynamics core of 1.9° latitude by 2.5° longitude and 26 vertical levels. The timestep was set to 30 min.

2.2.3 CO_2 simulations

To understand the role of fires in maintaining atmospheric CO_2 levels, CLM3 simulations were run with fires turned off. The experimental setup for this set of CLM3 simulations (Table 1) follows that of Kloster et al. (2012), also described in Sect. 2.1, with the exception that no fire disturbance was included. The spin-up procedure follows that used by Kloster et al. (2010). CLM3 begins with an initial non-zero carbon pool state and is integrated with the CN extension until the global average net ecosystem exchange (NEE) of carbon averaged over a 25-yr cycle of atmospheric forcing is less than $\pm 0.05\,\mathrm{PgC\,yr^{-1}}$. This is slightly less rigorous than the level used by Mahowald et al. (2011a) of $\pm 0.01\,\mathrm{PgC\,yr^{-1}}$ but consistent with Kloster et al. (2012). For the atmospheric forcing the Qian et al. (2006) reanalysis for 1948 to 1972 is looped and CO_2 is set at a preindustrial level. The spin-up lasted for 850 model years.

The transient run is branched from the end of the spin-up run starting at the year 1798 with pre-industrial CO_2 and PFT distribution. After 1798 the model setup uses the same transient CO_2, atmospheric forcing, and land-use change as the CLM3 runs described in Sect. 2.1. Therefore, changes in CO_2 from removing fires do not feedback into the CLM3 runs, and we assume that deforestation proceeds similarly whether fire is available as a vegetation-clearing tool or not. Since all ensemble members for the different future atmospheric forcings result in similar trajectories of fire emissions (Kloster et al., 2012), we chose one ensemble member from the CCSM and ECHAM groups to run for this analysis. Note that these CLM3 integrations are only used for the CO_2 RF computations and are not applied in any of the other RF analyses.

ACPD
12, 10535–10621, 2012

2.3 Radiative forcing computations

Radiative forcing is used as a tool for estimating the potential climate response to changes in various earth system constituents, including those with long timescale responses. The American Meteorological Society defines radiative forcing as a systematic perturbation to the flux of radiation at a certain level of the atmosphere. There are several ways to compute this quantity. Due to the diverse nature of forcing factors considered in the present study we used slightly different RF measures for the single forcings. In this study, the estimates for the RF of CO_2, CH_4 and N_2O follow the IPCC definition of adjusted radiative forcing, F_a (Ramaswamy et al., 2001). F_a is the change in radiative flux at the tropopause after allowing the stratospheric temperature time to adjust to the new forcing. The IPCC also defines radiative forcing as being relative to an initial preindustrial state. Here we use the term radiative forcing to refer to the forcing of a particular perturbation relative to the no-fire atmosphere.

Since we conducted the full chemistry CAM simulations with prognostic O_3 that did not feedback onto the model radiation, the calculated change in radiative flux at the tropopause due to O_3 from fires is better defined as an instantaneous forcing (F_i), which is how we report the RF of O_3 here. Hansen et al. (2005) report global climate simulations for the time period 1880 to 2000 for which the ratio of $F_i : F_a = 0.83$ for tropospheric O_3. While the exact ratio from Hansen et al. (2005) may not be applicable to our model experiment, their results suggests that F_i for O_3 from fires in this study is likely to be somewhat smaller but roughly equivalent to F_a.

For aerosols, the difference between the radiative fluxes at the tropopause and the top of the atmosphere (TOA) is considered small and the stratospheric adjustment for most aerosol forcings is minimal (Forster et al., 2007). Therefore the TOA RF computed in this study for aerosols can be compared to the F_a of the other forcings, assuming only small tropospheric temperature adjustments between simulations. For albedo changes we also report a TOA RF. The difference between F_i and F_a for surface albedo changes is considered negligible (e.g., Hansen et al., 2005; Randerson et al., 2006), but it should

ACPD
12, 10535–10621, 2012

be noted that differences in radiative fluxes between TOA and the tropopause are not accounted for here. Throughout the remainder of this paper, the radiative forcing for the various impacts of fire listed above will be referred to as RF. Details of the RF calculations are given in Appendix B.

3 Results

3.1 Carbon dioxide radiative forcing

Fires emit a large amount of CO_2 into the atmosphere. The estimates of global CO_2 emissions from fires in our CLM3 simulations range from 1.3 $PgC\,yr^{-1}$ for present day emissions to 2.4 $PgC\,yr^{-1}$ for the future trajectory with ECHAM atmospheric forcing. There is some evidence to suggest that fires may be a major source of the interannual variability in global CO_2 emissions (van der Werf et al., 2008; Nevison et al., 2008) although the short record of global fire activity limits the conclusions of such analyses.

Atmospheric CO_2 absorbs longwave radiation, trapping heat that might otherwise escape the atmosphere. It follows that emissions of CO_2 will lead to positive RF, and that fires will be a major contributor to that positive RF. However, in the case of fires, CO_2 emissions may be offset by the regrowth of vegetation in the burned area, which sequesters the lost C on time scales from a few years to many decades. Jacobson (2004) showed that, because of regrowth, the greatest current long-term source of CO_2 from fires comes from deforestation fires. When forests are cleared for agricultural land that has a relatively low capacity for C storage, the majority of the initially emitted C remains in the atmosphere or is sequestered by a different C sink. Deforestation fires are a net source of CO_2 to the atmosphere while it is often assumed that other fires are followed by regrowth of the same vegetation types and are neither a source nor a sink for CO_2 if fire frequency remains the same (e.g., Bowman et al., 2009). However, climate-induced changes to fire frequency will alter landscape-mean C stocks and affect atmospheric CO_2. In addition to these direct impacts on atmospheric CO_2, fires shape ecosystems

ACPD
12, 10535–10621, 2012

by altering population dynamics and species composition (Bond et al., 2005; Harrison et al., 2010; Rogers et al., 2011), affecting ecosystem productivity and decomposition rates. In these ways, fires act to control the C balance between the land and atmosphere.

In CLM3, the PFT distribution is not allowed to change due to fire disturbance. Future incarnations of CLM3 may include a dynamic vegetation response to fires and could show an even greater preindustrial C storage difference from fires as high-C forests replace the relatively low-C and fire-dependent grasslands in the no-fire case. Although, our other major assumption, that the atmospheric CO_2 remains constant with or without fires, would tend to buffer the increase in C storage when fires are removed as diminished atmospheric CO_2 would limit vegetation growth.

When fires are removed from the CLM3 model long-term integration, an additional ~500 PgC is stored in the land C pools (Fig. 4a, b, at year 1800), with contributions from increased storage in coarse woody debris (+31 %), litter (+17 %), and live vegetation (53 %). This sizeable preindustrial increase in land C storage due to removing fire activity corresponds to a new equilibrium atmospheric CO_2 concentration that has decreased by 41 ppm (details of this computation are given in Appendix B1). From this analysis we compute a RF of CO_2 from fire activity of 0.83 $W m^{-2}$. This forcing illustrates the important role fire disturbance plays in the global C cycle. Since fires are a relatively novel addition to current global models it is important to stress that many models could be missing this large forcing if they do not prescribe CO_2 concentrations.

In contrast to the CLM3 spin-up integration, 63 PgC was lost from the land C pools in the 19th and 20th centuries when fire activity was excluded from CLM3 (Fig. 4b). This results from land-use PFT changes (Hurtt et al., 2006) that are applied to the model starting in the year 1850, which we assume are identical between the two simulations. As forests are cleared and replaced by agricultural land, the no-fire simulation forests, which stored more C in the absence of fires, have more C to release (Fig. 4c). When fires were included, they maintained a lower C storing land surface, which was then a weaker C source when the land-use disturbance was applied. An interesting result of

ACPD
12, 10535–10621, 2012

the fire-caused decrease in C loss from land-use change is that the RF of CO_2 from fires in the year 2000 is negative, RF = $-0.21\,W\,m^{-2}$, compared to the preindustrial RF (using the pulse response method shown in Appendix B1). This means that since preindustrial times fires have reduced the amount of C available to be lost to the atmosphere through land-use change.

In the RCP 4.5 future scenario, land-use change decreases in magnitude after the year 2000 (Fig. 4c) while atmospheric CO_2 continues to increase in concentration and future climate anomalies are applied. Patterns and controls of land C storage between the fire and no-fire scenarios then begin to diverge. As temperatures increase, mobilization of soil N increases and plants are less N-limited, a result consistent with that of Thornton et al. (2009). However, the no-fire land surface begins to accumulate C at a higher rate than when fires are included. Without fires imposing consistent losses of C and N from vegetation (the no-fire simulation stores about 40 % more C in vegetation in 2000), gross primary production increases at a higher rate. The future increase in C storage for the no-fire simulation outpaces the increased availability of N for vegetation, leading to a more N-limited biosphere than in the fire simulation. The net balance, however, still favors increased C storage without fires.

When assessed in the year 2100, after an increase in the C storage in the no-fire simulation compared to the fire simulation, the RF from fire CO_2 is $-0.08\,W\,m^{-2}$ with the CCSM climate and $+0.08\,W\,m^{-2}$ with the ECHAM climate compared to the preindustrial RF. While the C storage in the no-fire land C pools increases rapidly toward the year 2100, the increased background CO_2 concentrations dampen the impact on the RF by the saturation effect. The magnitude and sign of the RF are also likely to be dependent on the choice of future land-use trajectory. RCPs 6.0 and 8.5 project considerably higher wood harvest rates globally compared to RCP 2.6 or RCP 4.5 which lead to a reduction in global biomass and contribute to a decrease in CLM3 fire emissions in the future by 30 % over RCP 4.5 (Kloster et al., 2012). If these alternative high harvest scenarios were applied to the current study, we would expect the RF from CO_2 between 1850 and 2100 from fires to decrease. It is difficult to quantify the uncertainty

ACPD
12, 10535–10621, 2012

in the RF for 2100 with respect to the different land-use change scenarios, but it can be said that the numbers given here for the year 2100 using RCP 4.5 are likely to be higher than if the other RCPs had been used.

3.2 Methane radiative forcing

Fires emit a small amount of CH_4 directly into the atmosphere but also affect the CH_4 mixing ratio by modifying the concentrations of important atmospheric oxidants. The major atmospheric sink for CH_4 is reaction with OH, and nearly 100 % of CH_4 removal occurs on the timescale of the primary, or longest-lived, mode (Wild and Prather, 2000). Previous modeling work by Naik et al. (2007) showed that fire emissions can lead to both increases and decreases in [OH] depending on the relative amounts of NO_x and CO + NMHC emitted. Increased emissions of NO_x, such as within a smoke plume, can enhance the production of O_3, which produces OH by photolysis (Naik et al., 2005). The enhanced production of OH leads to more destruction of tropospheric CH_4 and will decrease the CH_4 lifetime. In contrast, OH is removed from the atmosphere through oxidation of CO and NMHC for which fires are a major source. This acts to lengthen the CH_4 lifetime, counteracting to some extent the effect of increased NO_x.

Our method for computing the RF of CH_4 from fires can be found in Appendix B2. The magnitude of the RF due to CH_4 from fires is between 0.05 and 0.13 $W m^{-2}$ for all simulations (Table 2). In the present day, these fire RFs account for 9 % (CHEM_2000_KF) and 23 % (CHEM_2000_GF) of the global mean CH_4 RF, estimated by Forster et al. (2007). In the year 1850 simulations however, fires were responsible for a negative radiative forcing due to CH_4. The 1850 model troposphere saw enhanced OH production (Table 2) that outweighed the removal of OH by increased CO + NMHC. Therefore, these fires led to a global increase in [OH] and a decrease in [CH_4], in contrast with the other time periods (Table 2). This negative, indirect CH_4 forcing due to greater [OH] in the preindustrial case was large enough to counteract the positive RF from direct emission of CH_4 by fires and the RF from the increase in preindustrial tropospheric O_3.

ACPD
12, 10535–10621, 2012

3.3 Tropospheric ozone radiative forcing

Ozone is not emitted directly from fires but its concentration in the troposphere is often enhanced by the increase in O_3 precursor gases in biomass burning plumes (Pfister et al., 2008). Gas-phase fire emissions consist largely of CO and NMHCs and also include NO_x (Longo et al., 2009), all of which are important components in the photochemical production and loss of O_3. Pfister et al. (2006) modeled plume transport from boreal North American fires for the summer of 2004 and found enhancements of the lower tropospheric O_3 burden of about 10 % over Alaska and Canada. Production of O_3 within smoke plumes can continue for days and occur in distant locations relative to the fire. Real et al. (2007) simulated a net production of 22 ppbv O_3 in smoke from Alaskan fires with impacts on European air quality after long-range transport.

Here we consider the contribution of fires to the global annual mean tropospheric O_3 column burden for preindustrial, present and future fire emissions (Table 2). We define the chemical tropopause as the lower boundary of the lowest level with O_3 mixing ratio greater than 150 ppbv, as in Naik et al. (2007). They estimate a present day global O_3 burden of 30.1 Dobson Units (DU), which is slightly higher than our estimate of 27 DU, although, they use different biomass burning and anthropogenic emissions in their model as well as a coarser horizontal resolution. Lamarque et al. (2011) estimate the average annual global burden for 1991 to 2000 as 296 Tg O_3 defining the chemical tropopause at 100 ppbv O_3. Our figure for the present day, using their tropopause definition, is 273 Tg O_3, which is within the 10 % interannual variability range cited by Lamarque et al. (2011).

The preindustrial total O_3 burden estimated by CAM4 is less than half the present-day amount, but the proportional increase in O_3 burden due to fires is greatest for preindustrial emissions (Table 2). Past studies have shown that the addition of NO_x to a less polluted environment, which contains smaller background concentrations of NO_x and NMHCs, results in proportionally larger production of O_3 (e.g., Naik et al., 2005; Pfister et al., 2008). Background concentrations of NO_x and NMHCs were smaller in

ACPD
12, 10535–10621, 2012

the preindustrial emissions environment, prior to large anthropogenic impacts. Figure 5 shows the production of O_3 as a function of the increase in NO_x from fire activity at the surface in locations where fires occurred in the model. The preindustrial production efficiency of O_3 exceeds that of the other simulations by up to a factor of two, likely because of the pristine background environment.

Because of the relatively large impact of fires on the production of ozone in the pristine atmosphere, preindustrial simulations produce the greatest increase in O_3 and also the largest short-lived O_3 RF, 0.07 $W m^{-2}$ (Table 2; see Appendix B3 for RF computations). In the present-day and future, O_3 from fires are not a substantial short-term forcing on the radiation balance (Table 2).

Changes in tropospheric O_3 also perturb the primary mode CH_4 chemistry and can feed back onto O_3 concentrations on longer timescales (Naik et al., 2005, 2007). However, the primary mode response also leads to a small forcing and, combined with the short-term forcing, results in global, annual average O_3 RFs from fires between 0.03 and 0.06 $W m^{-2}$ (Table 2). The primary mode RF for preindustrial O_3 is negative due to the decrease in CH_4 lifetime caused by fires, which is detailed in the previous section. We compute a difference in global tropospheric O_3 RF from all sources (including the CLM3 fires) between 1850 and the present-day of 0.42 $W m^{-2}$, well within the range of model estimates for the instantaneous RF of O_3 reported by Forster et al. (2007).

Naik et al. (2007) estimate a present-day RF from fire produced O_3 of 0.11 $W m^{-2}$. They also find an increase of 10 % in tropospheric O_3 due to fires, in contrast to the 0–2 % global average increase in ozone for the present day simulated here. In an earlier study, Granier et al. (2000) estimate a 5 % increase in global tropospheric O_3 burden. While all three studies use different fire emissions, the O_3 production may not be a strong function of the fire emissions. The results shown here (see Fig. 5) suggest that the background chemistry modifies the fire emissions in producing the total O_3 change. Similar results were shown in a global chemical transport model by Fuglestvedt et al. (1999) who found increased O_3 in some regions when NO_x emissions

ACPD
12, 10535–10621, 2012

were systematically decreased. This occurred particularly in regions with high background NO_x concentrations.

3.4 Nitrous oxide radiative forcing

Fires produce small amounts of N_2O, considered the third most important greenhouse gas for future radiative forcing (Forster et al., 2007). The major global source of N_2O is denitrification by bacteria in soils and bodies of water. Since the preindustrial time period emissions of N_2O have increased, a change largely attributed to agricultural activities that increase the potential for denitrification in soils (Syakila and Kroeze, 2011). Estimates of annual global N_2O emissions from Meinshausen et al. (2011a) for 1850 and 2000, as well as future projections, are given in Table 3.

Using a box model (described in Appendix B4), we estimate the lifetime of N_2O for the case with all emissions, and use these parameters to estimate a lifetime without fire emissions. The difference between the two final state N_2O concentrations are small, and result in small, positive RFs (0.03 to 0.04 $W m^{-2}$) for preindustrial, present day and future time periods (Table 3).

3.5 Aerosol direct effect

Fires are the largest source of carbonaceous aerosols in the CAM5 simulations for all time periods (Table 4). The increase in annual average AOD due to fires is greatest for Central Africa and the Amazonian Basin, coincident with the areas of maximum fire activity (Fig. 6). Evidence of transport of aerosols upon easterly winds in the tropics can be seen in this figure with implications for the direct effect over often-cloudy marine environments. The modeled AOD increase (Fig. 6c with GFEDv2 emissions) matches well qualitatively and in maximum magnitude (~0.5) with the regional AOD change from removal of biomass burning season carbonaceous aerosols modeled by Sakaeda et al. (2011) for Central Africa. Increases in AOD are projected for the future time period particularly over South America, and Equatorial Africa (Fig. 6d, e).

ACPD
12, 10535–10621, 2012

The substantial impact on regional AOD suggests an important role for fire aerosols on the direct effect (details for computation of the direct effect of fire aerosols are given in Appendix B5). When only clear-sky is considered, the direct effect of fire aerosols is a negative forcing (Table 4). The values for future climates (AERO_2100_CKF and AERO_2100_EKF) are nearly double the preindustrial and present-day values using the CLM fire emissions, likely a result of the increased emissions over South America. If we include the direct effect of aerosols over clouds, the global annual average values become positive. This means that fire aerosols overlaying clouds have a substantial warming influence in our simulations. This can be estimated by subtracting the clear-sky direct effect from the all-sky direct effect using the values in Table 4. The magnitude of this effect on a global, annual average is large, between +0.25 and +0.5 $\mathrm{W\,m^{-2}}$ in our simulations. A qualitatively similar result was shown by Wilcox (2010) and Sakaeda et al. (2011) for Central Africa biomass burning aerosols.

The present-day values for the direct effect of fire aerosols from our study of +0.10 and +0.13 $\mathrm{W\,m^{-2}}$ (Table 4) fall within the confidence intervals of the IPCC Fourth Assessment estimate of $+0.03 \pm 0.12\,\mathrm{W\,m^{-2}}$ (Forster et al., 2007). Naik et al. (2007) reported a value of +0.13 $\mathrm{W\,m^{-2}}$ from their modeling study, as did Reddy et al. (2005). However, the appearance of strong agreement among model studies here should be met with some skepticism because, as pointed out by Naik et al. (2007) and Sakaeda et al. (2011), the direct effect depends largely on the model representation of cloudiness, which is generally inconsistent from model to model.

3.6 Aerosol indirect effects on clouds

The global average indirect effect from fire aerosols is dominated by decreases in the total cloud forcing (TCF) in regions off the west coast of Northern South America and Central Africa (Fig. 7). This suggests a globally important role for short-range transport of smoke from tropical fires on the easterly trade winds to near-coast marine stratocumulus cloud decks. Chuang et al. (2002) note that these clouds are particularly susceptible to changes in optical thickness from an influx of high aerosol number

ACPD
12, 10535–10621, 2012

concentration because of the low marine aerosol number concentrations. In our simulations, fire aerosols caused a two-fold increase in cloud droplet number concentration (CDNC) in the low clouds in some areas off the west coasts of South America and Central Africa, as well as approximately a 10 % decrease in cloud droplet effective radius in the same areas. Smaller droplet sizes enhance the cloud albedo, and lead to a more negative SWCF. This effect is also exacerbated by the persistent, high cloud fraction maintained by marine stratocumulus decks, particularly in the Northern Hemisphere summer (Hanson, 1991), which coincides with the season of greatest fire emissions in South America and Central and Southern Africa. A similar effect could explain the large negative cloud forcing in Northern Hemisphere high latitude regions caused by the GFEDv2 fire emissions (Fig. 7c). The CLM3 simulations do not capture the fire emissions at these latitudes.

Chuang et al. (2002) estimate an indirect aerosol forcing of $-1.16\,\mathrm{W\,m^{-2}}$ for carbonaceous aerosols from fires, although this estimate only includes the cloud albedo effect. The results from our simulations (Table 4) which include additional indirect effects such as effects on cloud height and lifetime, show comparable forcings, ranging between -1.74 to $-1.00\,\mathrm{W\,m^{-2}}$ (our method of computation is given in Appendix B5). Thus, our results also suggest that fires are particularly important for indirect cloud effects, even when compared to the global anthropogenic aerosol indirect effects. Fires do not account for as many particle emissions as anthropogenic activity in the present day (Andreae and Rosenfeld, 2008; Mahowald et al., 2011b), but this study suggests the contribution is still high due to the tropical location of the majority of emissions. Previous cloud parcel modeling work on Amazonian clouds has shown their albedo to be highly sensitive to intrusions of biomass burning aerosols (Roberts et al., 2003). Furthermore, the forcing from fire aerosols is not greatest directly over the areas where most fires burn, but is often imposed downwind and may depend largely on the affected cloud regime (Longo et al., 2009).

The aerosol indirect effect from anthropogenic activity (including fossil fuel burning, land use change and fires), defined as the difference in TCF between AERO_1850_KF

ACPD
12, 10535–10621, 2012

and AERO_2000_KF ($-1.76\,W\,m^{-2}$), is more negative compared to the estimates compiled by Forster et al. (2007). The disparity could result from our inclusion of additional indirect effects besides the cloud albedo effect, but more recent estimates of aerosol effects show that CAM5 tends to fall on the more negative side of the model spectrum (Quaas et al., 2009; Wang, M. et al., 2011). Therefore, we should note that our estimates for the indirect effects from fire aerosols might be more negative compared to future studies of a similar kind using other models. The indirect effect of aerosols is considered one of the most uncertain climate forcings in large part because of the difficult nature of simulating cloud processes which occur on a subgrid scale (Solomon et al., 2007). For example, the impacts of aerosols on tropical clouds are highly dependent on the extent of the convective development of the clouds (van den Heever et al., 2011), which is a subgrid-scale, parameterized process in our simulations and does not include explicit aerosol/cloud interaction that is only active for stratiform clouds.

Finally, in our simulations fires had a moderating influence on the indirect effects of anthropogenic aerosols between 1850 and 2000. That is, the magnitude of the indirect effect due to the change in aerosols from the year 1850 to the year 2000 is greater (more negative) when fire emissions are not included (difference between TCF_AERO_2000_KF minus TCF_AERO_1850_KF and TCF_AERO_2000_NF minus TCF_AERO_1850_NF) (Fig. 8). This could be the result of fire emissions "masking" part of the impact of anthropogenic emissions by adding to the background aerosol and diminishing the impact of further increases in aerosols on cloud droplet effective radius. This can also be seen in the general decrease in TCF from fire aerosols in 1850 and in 2000 (Fig. 7a, b). The preindustrial fire aerosol emissions, which are very similar in amount and distribution to the present-day (as predicted by CLM3), have a higher magnitude impact in general on the indirect effects. Since the present-day fires emit aerosols into what is, to varying degrees, a more polluted background, their impact might be dampened. In a similar sense, the fire emissions from 1850 and 2000 could dampen the impact of increased anthropogenic aerosol emissions on cloud processes and the overall indirect aerosol effect.

ACPD
12, 10535–10621, 2012

3.7 Deposition of aerosols onto snow and ice surfaces

The lifetime of aerosols in the atmosphere is on the order of days, after which they are removed either by dry deposition or by wet deposition in precipitation. When aerosols are deposited onto snow surfaces they can change its properties, with potential impacts on the albedo and even the melting rate of the snow (Flanner et al., 2007). The role of black carbon is particularly important because of its light-absorbing properties. Wang, Q. et al. (2011) found that more than half of the black carbon deposited onto Arctic sea-ice surfaces was from biomass burning, particularly in Russia. A similar result was reported by Stohl (2007) from modeling of BC transport.

The Snow, Ice, and Aerosol Radiative (SNICAR) model (Flanner and Zender, 2005, 2006) was run online in CAM5 to simulate changes in the RF of the snow surface due to fire aerosol deposition. Note that this analysis considers deposition of aerosols onto snow and ice surfaces over land but not over sea. The RF from deposition onto sea-ice is thought to be less important than deposition on snow/ice over land (Flanner et al., 2007), but if included, this may have increased the magnitude of our RF estimates. Differences in the annual average snow cover on land from simulation to simulation were minor (Fig. 9).

Bowman et al. (2009) estimated that the RF from fire-emitted black carbon depositing onto snow is negligible. Our simulations show a non-zero but very small RF (less than 0.01 $\mathrm{W\,m^{-2}}$) for preindustrial and present day fire emissions. The small impact is locally strongest in all time periods over the Himalayan Plateau (Fig. 9), the largest area of perennial ice cover near to tropical fires. This region has also been identified as important for radiative feedbacks from deposition of anthropogenic aerosols (Menon et al., 2010). Negative contributions to snow/ice albedo change RF (particularly visible in Mongolia and Northern China) came from decreased dust deposition through a dynamical feedback that we did not explore in detail.

While the RF is small, the efficacy of the black carbon deposition on snow forcing is large, estimated by Flanner et al. (2007) to be about three times greater than the

ACPD
12, 10535–10621, 2012

efficacy of long-lived greenhouse gases. This means that the climate response to this RF is greater than the response to an equal RF from the greenhouse gases. Flanner et al. (2007) explain that this results from surface albedo changes caused by accelerated melting of snow that contains absorbing aerosols, a process that is not captured by our methods.

Using observation-based emission estimates (AERO_2000_GF) results in the highest globally averaged RF from aerosol deposition on snow due in part to greater contributions from high latitude Asian fires. This is consistent with the higher carbon emissions in Northern Asia in GFEDv2, discussed previously (Sect. 2.1.1).

3.8 Local albedo changes

Fires have a direct impact on the albedo of the land surface by removing or altering vegetation cover, charring the surface, and in the case of forests, by exposing underlying surfaces with different albedos (grasses, snow, etc.). While extreme local changes in albedo have been observed, the impact is limited in scale to the area burned and may not be as important on a global average (Randerson et al., 2006). Here we use our model results and post-fire land surface albedo change curves compiled from the literature to estimate the RF of the albedo changes and the change in the RF through time (see Appendix B6 for details).

The temporal evolution of the estimated RF shows the strong seasonality of the forcing (Fig. 10). To estimate the total impact of yearly fires, which can persist for years, we sum the yearly global RF from land surface albedo change and assume the fire return time exceeds the albedo recovery time. The total RFs from surface albedo changes from fires were $-0.19\,W\,m^{-2}$, $-0.18\,W\,m^{-2}$, and $-0.24\,W\,m^{-2}$ for 1850, 2000, and 2100, respectively, with the year 2100 figure being the average between the two future simulations. When the GFEDv2 emissions are used, the smaller proportion of mid-latitude forest fires in this inventory (Fig. 3c) leads to a reduced impact of surface albedo changes and a RF of $-0.10\,W\,m^{-2}$. The impact of increased snow exposure in burned areas during the Northern Hemisphere winter is evident in the monthly time-

ACPD
12, 10535–10621, 2012

series detail in Fig. 10 and also in the biome-specific RFs shown in Fig. 11. In the months of March and April the RF decreases as Northern Hemisphere solar insolation increases and some exposed ground is still snow-covered.

The net radiative forcing of fires, integrated over different time periods, highlights the strong warming immediately after fires from surface albedo (Fig. 11). The global average forcing then becomes negative after six months as extratropical forest fires, the majority of which occur in the local summer season, have left behind open canopies that expose high albedo snow surfaces to the sun. The albedo in areas of burned tropical forests have also increased after six months.

Bowman et al. (2009) estimate the difference in RF from fire-caused surface albedo changes between 1750 and 2000 to be $-0.10\,\mathrm{W\,m^{-2}}$, computed as half of the total land-use related surface albedo change reported by Forster et al. (2007). Our value for RF change from 1850 to 2000 is small and has a positive sign ($+0.01\,\mathrm{W\,m^{-2}}$). The positive change from our analysis for this period is a result of the conversion of forests to crops that took place over the 19th and 20th centuries. CLM3 fires in the year 2000 burned proportionally fewer forests and more crops than in 1850 (Fig. 3c). Since crops are grouped in with grasses for our albedo analysis, there is a stronger initial warming from grasses for 2000. In 2100, an increase in total forested area burned leads to more long-term cooling (Fig. 11) and overall greater cooling than in 1850 or 2000.

3.9 Aerosol indirect effects on biogeochemistry

Fire aerosols not only impact climate directly, but can cause an indirect effect on climate through biogeochemical cycles, especially the carbon cycle (Mahowald, 2011). There are two ways that fire aerosols can impact biogeochemistry, first through adding nutrients (or pollutants) and secondly through modifying climate. Fire gases and aerosols contain N and phosphorus (P), which can fertilize downwind nutrient limited forests (e.g., Vitousek, 1984; Mahowald et al., 2005; Chen et al., 2010). It has been speculated that the increased P in ash in the Amazon due to increased biomass burning

ACPD
12, 10535–10621, 2012

has contributed to the larger uptake of carbon observed during the 1980s and 1990s, resulting in a radiative forcing of between 0 and $-0.12\,W\,m^{-2}$ (Mahowald, 2011).

N deposition from anthropogenic sources is thought to be increasing the drawdown of CO_2 from terrestrial ecosystems causing a forcing of between −0.24 and $-0.74\,W\,m^{-2}$ (Mahowald et al., 2011b): only half of that is in the aerosol form, but for this problem both gas and aerosol impacts on biogeochemistry are important. The ratios of N emissions from fire (computed from the CLM3 simulations) to present day anthropogenic emissions (Lamarque et al., 2010) are 11 %, 9 % and 15 % in 1850, 2000 and 2100 (averaged between the two ensemble future simulations). If this impact were linear on the N deposition, this would imply between −0.02 and $-0.08\,W\,m^{-2}$ from the fertilization of land due to fires in the preindustrial, with very similar values (within the uncertainties) for current and future values.

Fire aerosols are also thought to contain soluble iron (Fe) (Guieu et al., 2005), an important micronutrient for ocean biogeochemistry (Martin et al., 1991). Estimates of the increased uptake of CO_2 in the oceans, from both increases in the solubilization of Fe (due to fossil fuel sulfur dioxide emissions, industrial combustion soluble Fe and biomass burning soluble Fe), suggest a reduction in the CO_2 of 2 ppm (Krishnamurthy et al., 2009). If we assume up to half of this is from fires (which is likely to be an overestimate), this results in a radiative forcing of $0.02\,W\,m^{-2}$, a small number. While atmospheric deposition of Fe, N and P are likely to impact the budgets and cycles within the oceans, the impacts in terms of CO_2 of increased N and P deposition onto the ocean are thought to be smaller (Krishnamurthy et al., 2010).

Finally the climate impacts of fires can themselves, through potential climate response, impact the carbon cycle and feedback onto climate (e.g., Jones et al., 2001; Mahowald, 2011; Mahowald et al., 2011a, b). The impact of climate onto biogeochemistry, even the carbon cycle, is not well understood (Friedlingstein et al., 2006; Friedlingstein and Prentice, 2010; Mahowald et al., 2011a), however estimates from coupled-carbon-climate models suggest a roughly linear response with climate forcing of between 0 and 40 ppm of CO_2 for a $1.4\,W\,m^{-2}$ RF (Mahowald et al., 2011a). This global

ACPD
12, 10535–10621, 2012

forcing of fires is referred to as the climate-BGC feedback in the following discussion. The climate-BGC feedback RF is estimated by applying the linear response relationship between CO_2 and climate forcing to the sum of all RFs of fires as estimated by this study (not including the climate-BGC feedback being computed here). This forcing is separate from other fire forcings involving the C cycle such as the BGC effects of aerosols and the direct impact of fires on atmospheric CO_2 concentrations. Using this method, we estimate values of the fire climate-BGC feedback RF of $-0.26\,W\,m^{-2}$, $-0.09\,W\,m^{-2}$ and $-0.10\,W\,m^{-2}$ for the preindustrial, present day and 2100 time periods, respectively.

4 Conclusions

Comprehensive assessment of the role of fires in climate is challenging because of the complex nature of the numerous fire/earth system interactions (Fig. 1). While previous studies have included rough estimates of the effect of fire on climate, or only a subsample of processes (e.g., Naik et al., 2007; Bowman et al., 2009; Pechony and Shindell, 2010; Stone et al., 2011), here we make detailed calculations of the impact of fire on the earth's simulated radiative budget. In this study we applied several different analysis techniques to the results of CAM and CLM simulations to estimate the RF of fire through impacts on CO_2, CH_4, N_2O, O_3, aerosol direct and indirect effects (on clouds and biogeochemistry), snow/ice and land surface albedo, and the climate-BGC feedback. We used emissions inventories from time periods centered on 1850, 2000 and 2100 to examine how the RF of fires has changed since preindustrial times, and how it may change in the future (Fig. 12, 13; Table 5).

We compared the RFs calculated using the prognostic fire in the earth system model (Kloster et al., 2010) to the GFEDv2 inventory, which suggest that there are still gaps in model estimates of the distribution of fires and a need for improvement. Continued progress in the development of fire emission inventories based on satellite observations, such as the GFED (van der Werf et al., 2010), is essential for model validation.

ACPD
12, 10535–10621, 2012

Within the model, prognostic burn severity may be the next major step toward better matching the predicted fields to the inventories. Future modeling work on fire impacts would also benefit from dynamic vegetation that captures the succession of different PFTs following fire and the evolution of different fire regimes since we have shown that changes in landscape and vegetation caused by fires significantly contribute to the overall fire RF as do fire emissions of aerosols and greenhouse gases.

Figure 12 shows the RF due to fires for all impacts assessed in this study for preindustrial conditions. The change in all RFs between 1850 to 2000 and 1850 to 2100 are illustrated in Fig. 13 with the range in RF between the two future atmospheric forcing datasets shown. Immediately obvious in Fig. 12 is the dominant, and partially canceling nature, of the CO_2 and aerosol indirect effect RFs in the preindustrial emissions environment. We made several assumptions to estimate the CO_2 RF (see Sect. 2) and the other dominant RF, the indirect aerosol effect on clouds, is highly uncertain in model predictions. The IPCC AR4 use a range of confidence of $1.5\,W\,m^{-2}$ to bound their estimates for the first anthropogenic aerosol indirect effect (Forster et al., 2007). Nevertheless, our results for preindustrial times identify the major radiative forcing contributions of fires (totaling $-1.19\,W\,m^{-2}$), demonstrating their role in a more naturally-forced global environment.

The decreases in fire-induced RF by CO_2 and O_3 from 1850 to 2000 are notable in that they may have been unexpected (Fig. 13). In our simulations, by maintaining reduced carbon stocks in the earth's forests, fires limited the amount of CO_2 that was released by the conversion of forests to agricultural land that took place during the 19th and 20th centuries. In the case of O_3, higher background concentrations of NO_x in the present day model environment lead to a decreased O_3 production efficiency and decreased RF. The relative decrease in O_3 may have contributed to the extended lifetime of CH_4 in the present day, changing the sign of the CH_4 RF from negative in preindustrial to positive and compensating for the decreased RF of O_3.

The largest change in fire RF from 1850 to 2000 was caused by the aerosol indirect effect, which increased by $0.6\,W\,m^{-2}$ using the CLM fire emissions. While emissions

ACPD
12, 10535–10621, 2012

from fires during the two time periods were similar in magnitude (Fig. 2) and in geographical distribution (Fig. 3), the impacts of present-day fire aerosols onto clouds are somewhat reduced by higher background aerosol number concentrations. The effect of the polluted present day atmosphere is to mask the additional forcing from natural aerosols, such as from fires. Largely due to the influence of the aerosol indirect effect, the overall RF of fires estimated by the model simulations increased by about 0.7 $W m^{-2}$ from 1850 to 2000. This suggests, in other words, that anthropogenic activities have caused the cooling potential of global modeled fires to decrease by 56 % since 1850 even with very little trend in modeled fire emissions during this time.

From years 2000 to 2100, the projected fire emissions depend on the projected climate change applied as atmospheric forcing (e.g., Kloster et al., 2012). Both ensemble CLM3 simulations project an increase in fire emissions into the future; however, the increase is modest for the CCSM atmospheric forcing and sizeable for the ECHAM forcing (see Fig. 2, Kloster et al., 2012). These projections give some sense of the range in predicted fire activity in the future. We use the differences between the results of the two projections as bounds on our RF estimates for the future (Fig. 13). The high fire emissions projection (ECHAM forcing) leads to a CO_2 RF that is comparable to the preindustrial value as greater amounts of carbon are lost to the atmosphere by burning but the impact is buffered by the CO_2 saturation effect. The positive direct effect of aerosols is also enhanced by the greater fire emissions by 0.13 $W m^{-2}$ over the CCSM driven atmospheric forcing results. However, by substantially increasing fire aerosol emissions toward the year 2100, the ECHAM-forced scenario was ~0.3 $W m^{-2}$ below the CCSM-forced scenario in the estimate of the RF from aerosol indirect effects. Altogether, the two very different future fire emissions scenarios lead to similar total fire RFs. The magnitude of the model-predicted year 2100 fire RF has decreased somewhat from the present-day, being about 0.4 $W m^{-2}$ greater than the 1850 value (Fig. 13).

Past modeling studies have found that different forcing agents may have different climate sensitivities, known as efficacies when defined in relation to the climate sensitivity

ACPD
12, 10535–10621, 2012

of CO_2 forcing (Hansen et al., 2005; Solomon et al., 2007). The values from Hansen et al. (2005) are given in Table 5. In addition, it is worth mentioning that because fires are spatially variable, the climate response to associated forcings is likely to vary considerably between regions. This is especially likely for forcings from short-lived gases and aerosols, as well as surface albedo changes and biogeochemical effects.

The uncertainties in net radiative forcing of fires are large and difficult to quantify, including major uncertainty in the total fire emissions, spatial variability of emissions, the model representation of clouds, the trajectory of land-use and future atmospheric constituents and forcing onto the land surface, and the role of nitrogen in the land model. Important processes, such as dynamic vegetation and ocean biogeochemistry, were not included in these simulations. Still, major lessons can be learned from these results. We found that the background environment into which fires emit aerosols and trace gases can be just as important, if not more, than the magnitude of the emissions. Also, the effects of fires onto ecosystems by moderating C storage were a major forcing on the atmosphere. Therefore, we conclude that anthropogenic impacts on fire activity, igniting and suppressing fires, are not the only paths by which humans can affect the climate forcing from fires. Instead, fires as a process are highly integrated within the Earth system and respond to changes whether from natural or anthropogenic sources. Comprehensive model representations of the Earth system, therefore, must include the effects of fires on the climate and preferably, the effects of climate on fires and fire impacts as well.

Appendix A

Scaling of aerosol emissions in CAM5

Recent studies suggest that GFEDv2 bottom-up estimates of carbon emissions from biomass burning in tropical regions, especially South America, may be biased low when compared to satellite, surface, and airborne observations of aerosol optical depth at a

ACPD
12, 10535–10621, 2012

wavelength of 550 nm (AOD_{550}) (e.g., Bian et al., 2007; Chin et al., 2009). To compensate for this apparent bias, the modeled AOD_{550} based on the GFED emissions is scaled to match a dataset or combination of datasets of observed AOD_{550} (e.g., Nevison et al., 2008; Matichuk et al., 2008). For example, Matichuk et al. (2008) compare the AOD_{550} retrieved by satellites and observed by AERONET to model predictions of the same quantity using GFED emissions. By examining selected sites in the Amazon region and for days with large aerosol contributions from biomass burning they found that it was necessary to scale the emissions source function by a factor of six to match the observed AOD_{550}. Such a large discrepancy could result in part from an inaccurate wet deposition parameterization, but Matichuk et al. (2008) also note the large uncertainties in the GFED burned area product, particularly in deforestation fire regions, and the uncertainties in the emission factors for various chemical species as defined by Andreae and Merlet (2001).

Scaling of biomass burning emissions in our study follows the method of Johnston et al. (2012) with only slight modifications. This method is different from previous schemes as it identifies high-fire locations, and low-fire and high-fire seasons, and scales the AOD for each separately. In this way the influence of the background aerosols on the overall scaling, noted as a source of uncertainty for this process by Matichuk et al. (2008), is reduced. We performed two additional 5-yr simulations with CAM5 and MAM3 to optimize aerosol emissions. These simulations were identical to AERO_2000_GF and AERO_2000_NF but used the un-scaled GFEDv2 emissions averaged over the period 1997–2002. We define an AOD_{CAM} as the 5-yr average monthly mean AOD_{550} from the simulation with GFED fire emissions and AOD_{NOFIRE} as the 5-yr average monthly mean AOD_{550} from the simulation with no fire emissions. AOD_{FIRE}, defined as the difference between AOD_{CAM} and AOD_{NOFIRE}, is considered to be the model estimate of AOD_{550} resulting from fire emissions.

The model data were scaled using observations from the Moderate Resolution Imaging Spectroradiometer (MODIS) and Multi-angle Imaging Spectroradiometer (MISR) instruments as well as ground based observations from the Aerosol Robotic Network

ACPD
12, 10535–10621, 2012

(AERONET). Monthly mean values of AOD_{550} were derived from satellite retrievals from the years 2000 to 2009, and also from the full record of each AERONET station with data for at least one yearly cycle. Since we are comparing monthly climatologies, and these may be averaged over different time periods, we expect to introduce some error related to the interannual variability of fires. However, the variability in fire emissions from year to year is low in Africa and South America (van der Werf et al., 2006) where the largest amounts of fire emissions occur.

The results of a regression analysis of the model and satellite AOD data onto the AERONET observations for all station locations are given in Table A1. Both model and satellites underestimate AOD when compared to AERONET as shown by the slope of the regression line, although the satellite retrievals show less spread about the line. Where AOD is reported less than 0.2 by MODIS the observation is removed following the recommendation of Hyer et al. (2011) who note that the low-AOD observations approach the signal to noise threshold. For satellite retrievals a separate slope is computed where the regression line is given a y-intercept of zero. Hyer et al. (2011) also found non-zero intercepts when regressing AERONET AOD data onto the MODIS dataset and writes that these are often caused by retrieval errors. The same adjustments are made to the MISR data.

Kahn et al. (2005) compare MISR retrieved AOD to AERONET observations and find much better agreement. However, they made comparisons for individual satellite passes, whereas we are inclined to use monthly climatologies. We expect the differences between our analysis and that of Kahn et al. (2005) are due to this averaging. Nevertheless, because the model AOD is more similar to the satellite AOD than either of them are to the AERONET data, we perform an adjustment to the satellite AOD data prior to the scaling of the model AOD. The satellite estimates of AOD_{550} are prepared by simply applying the slope adjustment factors given in Table A1. These are computed to adjust the slope of the regression line between the MODIS and MISR AOD and the AERONET AOD to one.

ACPD
12, 10535–10621, 2012

The regions for scaling were defined as the 1/3 of the area within each of the 14 GFED-defined regions (van der Werf et al., 2006) with the highest value of AOD_{FIRE}. All of the following computations are done on these 14 sub-regions. Fire emissions are largely seasonal (van der Werf et al., 2006) making it possible to designate a fire season, defined as the four months out of an annual cycle with the highest monthly mean value of $AOD_{FIRE} : AOD_{NOFIRE}$, and a no-fire season, defined as the four months with the lowest mean ratio, for each sub-region. The AOD_{CAM} averaged over each region for the no-fire season months, as well as the AOD_{550} estimates from MODIS and MISR for the same months and same regions, are used to compute a scaling factor for the background aerosol, β, using this expression adapted from Johnston et al. (2012):

$$AOD_{satellite} = \beta \cdot AOD_{NOFIRE} + AOD_{FIRE} \quad \text{(A1)}$$

The scaling factor β was chosen to satisfy this relationship for all 14 sub-regions. Note that β is used only for computation of α and is not applied to the model emissions. Using β, the fire emissions scaling factor, α, is chosen to satisfy the following expression for the fire months (adapted from Johnston et al., 2012):

$$AOD_{satellite} = \beta \cdot AOD_{NOFIRE} + \alpha \cdot AOD_{FIRE} \quad \text{(A2)}$$

We applied the results of this analysis to regions that emit greater than 100 Tg C annually from biomass burning (scaling factors given in Table 2). These were Southern Hemisphere South America (SHSA), Northern and Southern Hemisphere Africa (NHAF, and SHAF, respectively), boreal Asia (BOAS), southeast Asia (SEAS), equatorial Asia (EQAS), and Australia (AUST). The average of α computed for MODIS and MISR is used to approximate a scaling factor for fire emissions in the high-fire emission regions. Matichuk et al. (2007) found that varying the initial mass of biomass burning emissions led to linear variations in the resulting AOD_{550}. Therefore the scaling factor is directly applied to the model emissions. The impact of applying the scaling factors to the model emissions was assessed with an additional G_FIRE_2000 5-yr simulation using the scaled GFEDv2 emissions. The results of this simulation are shown in Fig. A1

ACPD
12, 10535–10621, 2012

in comparisons of the model and AERONET AOD_{550}. The regions SHAF, SHSA, and EQAS have the highest fraction of model AOD from fires and see the largest increase in model AOD (note that the results for EQAS are not plotted due to the very small number of AERONET stations in this region). The change is less visible in the other regions where either the scaling factor was set to one, or where fires do not contribute significantly to the model AOD. In all cases the model AOD is still low compared to the AERONET monthly values. Overall, the scaling more than doubled fire aerosol emissions globally (increase of 106 %) using the scaling of the GFEDv2 emissions as an example. The increase in fire aerosol emissions resulted in a 7 % increase in global, annual averaged AOD from all aerosols (magnitude increase of 0.01) again using the GFEDv2 emissions.

Reaching agreement between the models and observations of AOD in biomass burning regions is a work in progress. Koch et al. (2009) suggest improving model treatment of the aerosol mixing state and optical properties of light-absorbing aerosols in addition to updating emissions inventories with information about aerosol size and light-absorbing ability. The method of scaling that we described here does not further these aims but simply applies a patch to the emissions used in our model runs to push their representations of atmospheric aerosols closer to observations.

Appendix B

Radiative forcing calculations

B1 Carbon dioxide

Here we examine the redistribution of C between land, atmosphere and ocean pools that occurs because of fire activity. The redistribution is quantified as the difference in total C stored in soil, vegetation and plant litter between the fire and no-fire land surface, simulated with CLM3. It is worth reiterating that atmospheric CO_2 forcing was

ACPD
12, 10535–10621, 2012

identical for the fire and no-fire integrations of CLM3, disregarding feedbacks between CO_2 changes due to the removal of fires, and growth of vegetation.

To estimate the amount of CO_2 that is in the atmosphere as a result of fire activity for the three time periods in question, we assume that the difference in total land storage of C between the fire and no-fire CLM3 simulations was emitted to the atmosphere. Deforestation fires do not contribute to this difference in CLM3 since we apply the same land-use change regardless of whether fire was used as a tool for clearing or not. CO_2 sequestered by the regrowth of vegetation in fire-affected areas is accounted for in the C storage difference. This is illustrated in Fig. B1 where the CO_2 sequestered when fires are removed is marked as $[CO_2]_s$ and represents figuratively the amount of CO_2 that remains in the atmosphere because of fires.

The removal rate of CO_2 from the atmosphere is buffered by physical processes that are themselves dependent on the carbon concentrations in the atmosphere and ocean (Archer et al., 2009). Therefore, to estimate the "no-fire" atmospheric CO_2 concentration for the preindustrial time period, we compute a new steady-state land-atmosphere-ocean C partitioning accounting for the change in land C storage predicted by CLM3. This steady-state can be imagined to have taken place over a long enough timescale for the three main C pools to reach equilibrium and can be considered a natural state, or the state of the C-cycle prior to anthropogenic C emissions. Goodwin et al. (2007) introduce an analytical expression for the change in atmospheric CO_2 at equilibrium with the ocean and land, given a perturbation to an initial C pool partitioning:

$$P_{CO_2} = P_i e^{\frac{\Delta \Sigma C}{I_B}} \quad \text{(B1)}$$

where P_{CO_2} and P_i are the new steady-state and initial atmospheric CO_2 concentrations, respectively, $\Delta\Sigma C$ is the total change in C stored on land, and I_B is a steady-state, preindustrial total C inventory for which we use $I_B = 3100\,\text{GtC}$ as suggested by Goodwin et al. (2007). The new concentration can be considered the $[CO_2]_s$ (from Fig. B1), or the amount of C in the steady-state, preindustrial atmosphere due to global fire activity.

ACPD
12, 10535–10621, 2012

To estimate the concentration of CO_2 in the atmosphere because of fire emissions that took place against a background of changing anthropogenic C emissions (i.e. 1850 through 2100), we use a pulse response approach for atmosphere-ocean C equilibrium, similar to Randerson et al. (2006). If we conceive that the land surface C storage prevented by yearly, global fires is emitted annually as a pulse of CO_2 we can estimate the airborne fraction of the pulse after the given time period using a pulse response function. Enting et al. (1994) generated CO_2 pulse response functions from several models including the ocean-carbon model introduced by Siegenthaler and Joos (1992). They defined coefficients for the response function given preindustrial CO_2 parameters (IINIT), for emissions sustaining 1990 CO_2 concentrations (IP90), and for an emissions scenario leading to a CO_2 concentration of 650 ppmv by the year 2100 (IPERT). To estimate the concentration of CO_2 in the atmosphere from fires for the present and future time periods, we calculate a yearly pulse from the model output where CO_2 pulse amounts are considered to be equivalent to the yearly change in the difference in global total C between the fire and no-fire land surfaces. Then we apply the response function to compute the airborne fraction of the yearly pulse at the assessment year (either 2000 or 2100), multiply each pulse by the corresponding airborne fraction, and sum these results over the given time period.

In this sense, we are assessing the change in atmospheric CO_2 relative to the preindustrial state from fires that occurred before 2000, for present day, and before 2100 for the future. The IP90 response function is applied to these pulses yearly from 1850 to 1990 and IPERT is used from 1990 to 2100. IP90 was designed assuming present day background CO_2 concentrations initially, meaning it is not directly applicable to the problem of increasing CO_2 concentrations from 1850 to 1990. Therefore for comparison, we repeated the analysis using the constant airborne fraction estimated by Knorr (2009) over this period (f = 0.43), which resulted in a 30 % decrease in the computed RF. The disadvantage of this approach is that the airborne fraction for more recent years is weighted the same as for years in the distant past.

ACPD
12, 10535–10621, 2012

After calculating the new atmospheric CO_2 concentration, the Ramaswamy et al. (2001) simple expression for estimating the RF of CO_2 was used for the final step in the calculation.

$$\Delta F = 5.35 \cdot \ln\left(\frac{C}{C_0}\right) \quad \text{(B2)}$$

This function, in which C is the perturbed atmospheric CO_2 concentration and C_0 is the CO_2 concentration in the unperturbed state, both in ppm, captures the impact of the CO_2 saturation effect by which higher ambient concentrations of CO_2 act to diminish the RF of additional CO_2 inputs.

B2 Methane

The global mean lifetime of CH_4 in the present-day troposphere with respect to reaction with OH is estimated to be between about 8 to 10 yr (Fuglestvedt et al., 1999; Dentener et al., 2005). Due to this long lifetime in the troposphere, CH_4 impacts on RF cannot be explicitly calculated from a single year model simulation. Instead, a change in [OH] (assumed to be the dominant sink for CH_4) is used to compute a new CH_4 lifetime from which a "steady-state" [CH_4] and associated RF can be estimated (Fuglestvedt et al., 1999). Here we apply the Osborne and Wigley (1994) CH_4 mass-balance method with slight modifications that account for the perturbation lifetime (Wild and Prather, 2000), and for the RF of the direct CH_4 emissions from fires. Osborne and Wigley (1994) define the methane mass balance as,

$$d[CH_4]_o/dt = E_o/\beta - [CH_4]_o/\tau_o \quad \text{(B3)}$$

where $[CH_4]_o$ is the observed or predicted global mean surface concentration, t is time, E_o is the total emission of methane from all sources, $\beta = 2.75$ is a proportionality constant, and τ_o is the methane lifetime considering all sources. The lifetime, τ, is computed from the model global mean [CH_4] and [OH] below 200 hPa for all CHEM

ACPD
12, 10535–10621, 2012

simulations, and using the temperature dependent reaction rate constant from Seinfeld and Pandis (2006). If we assume a steady-state for $[CH_4]$ (i.e. $d[CH_4]_o/dt = 0$), the following expression results.

$$E_o = \frac{[CH_4]_o \beta}{\tau_o} \tag{B4}$$

Next, to estimate the change in $[CH_4]$ due to removing fires, $\Delta[CH_4]$, for the model-calculated change in τ due to removing fires, $\Delta\tau$, at a new steady-state, we use E_o from Eq. (B4) in the following expression adapted from Naik et al. (2005):

$$\Delta[CH_4] = F \cdot E_o \cdot \Delta\tau \tag{B5}$$

The parameter F accounts for the positive feedback between $[CH_4]$ and [OH] that occurs on the primary mode timescale (Wild and Prather, 2000; Fiore et al., 2009). It can be defined as the ratio of the adjustment time for $[CH_4]$ after a perturbation to the mean $[CH_4]$ lifetime. Here we use $F = 1.4$ as recommended by Prather et al. (2001).

Finally, the impact of direct emissions of CH_4 from fires on steady-state $[CH_4]$ is computed separately using the change in CH_4 emission caused by removing fires, ΔE, and a form of the mass balance Eq. (B3) from Osborne and Wigley (1994) (their Eq. 11), where F is used to represent the ratio of the perturbation lifetime to the initial lifetime:

$$\Delta[CH_4] = F \cdot \frac{\Delta E}{E_o} \cdot [CH_4]_o \tag{B6}$$

The changes in $[CH_4]$ due to the removal of fires, both from modifying the oxidant distribution of the atmosphere and from reducing direct CH_4 emissions, are then added together to give the steady-state no-fire CH_4 concentration, $[CH_4]_{nf}$. The global mean RF due to CH_4 from fires for each time period is then considered to be the difference in total RF between $[CH_4]_o$ and $[CH_4]_{nf}$. The RF computation follows the method given

ACPD
12, 10535–10621, 2012

by Ramaswamy et al. (2001):

$$\Delta F = 0.036\left(\sqrt{M} - \sqrt{M_o}\right) - \left[f(M, N_o) - f(M_o, N_o)\right] \quad \text{(B7)}$$

$$f(M, N) = 0.47 \ln\left[1 + 2.01 \cdot 10^{-5}(MN)^{0.75} + 5.31 \cdot 10^{-15} M (MN)^{1.52}\right] \quad \text{(B8)}$$

where M and N are average tropospheric concentrations of CH_4 and N_2O (in ppb), respectively, and M_o and N_o are the concentrations of those species in the unperturbed state.

B3 Tropospheric ozone

To assess the global mean RF due to tropospheric O_3 from fires for each simulation, the CAM4 radiation package was run offline using the Parallel Offline Radiative Transfer (PORT) tool for CAM. PORT applies the CAM radiative transfer scheme to a time-slice of the atmospheric state predicted by CAM allowing for sensitivity analyses that cannot be run online.

Radiative transfer calculations are carried out with PORT for the instantaneous model atmospheric state at 36.5-h intervals. In this way, the offline radiation diagnostics are computed for the entire diurnal cycle every 48 model days. The calculations are run a second time with O_3 removed below the instantaneous model-defined chemical tropopause. Then the net radiative flux at the instantaneous model-defined tropopause is averaged over the globe and the entire time-series (one year) to provide an estimate for the RF of tropospheric O_3. The contribution from fires is defined as the difference in tropospheric O_3 RF between the CAM simulations with fire emissions and the simulations without fire emissions.

The direct influence of fires on O_3 concentration through the emission of short-lived precursors (NMHCs and NO_x) has been called the "short-lived" RF of O_3 by Naik et al. (2005). A second O_3 RF arises from perturbations to the CH_4 concentration that take place over longer timescales. As CH_4 responds to changes in OH, the production

ACPD
12, 10535–10621, 2012

of peroxy radical concentrations is modified, which then feeds back onto the O_3 concentration (Naik et al., 2005). This primary mode response in O_3 can be approximated by the following expression from Naik et al. (2005):

$$(\Delta O_3)_{\text{primary}} = \frac{\Delta[CH_4]}{[CH_4]} \cdot \frac{0.64}{0.1} \text{DU} \quad \text{(B9)}$$

The column O_3 response of 0.64 Dobson Units (DU) for a 10 % change in CH_4 was approximated from model results (Prather et al., 2001). The RF of the primary mode response is estimated with the recommended value of O_3 forcing per DU from Forster et al. (2007) of $0.032 \pm 0.006\,\text{W m}^{-2}\,\text{DU}^{-1}$.

B4 Nitrous oxide

Emissions of N_2O from fires are estimated in this study using the CLM3 FIRE_CLOSS and the emission factor for N_2O from Andreae and Merlet (2001). From this analysis, fires contribute between 2 % to 5 % of global N_2O emissions for each time period (Table 3). The present-day value for global fire emissions of N_2O from CLM3 ($0.4\,\text{Tg N}(N_2O)\,\text{yr}^{-1}$) is slightly below the range of previous estimates, 0.5 to $1\,\text{Tg N}(N_2O)\,\text{yr}^{-1}$ (Cofer et al., 1991; Ramaswamy et al., 2001; Syakila and Kroeze, 2011).

The main sink for N_2O is destruction by photolysis in the stratosphere. In the troposphere, N_2O is inert and nearly uniformly distributed. Montzka et al. (2003) estimated an N_2O lifetime in the atmosphere of 114 yr for the present day concentration. Its long residence time partly accounts for the importance of N_2O as a greenhouse gas despite its low concentrations relative to CO_2. More recent work has suggested a century-long timescale relationship between N_2O and CH_4, combining stratospheric and tropospheric chemistry that has implications for our understanding of the N_2O lifetime (Prather and Hsu, 2010).

To determine the contribution of fires to N_2O concentrations we use a simple atmospheric box model. The box model assumes that the change in N_2O concentration with

ACPD
12, 10535–10621, 2012

time equals the difference between total N_2O emissions and N_2O loss. It is expressed by Kroeze et al. (1999) as,

$$\frac{dC}{dt} = \frac{S}{F} - \frac{C}{\tau} \tag{B10}$$

where C is the N_2O concentration (ppbv), S are N_2O emissions ($TgN\,yr^{-1}$), F is a conversion factor ($4.8\,TgN\,ppbv^{-1}$), t is time (yr), and τ is the N_2O lifetime (yr). We account for the feedback of the changing N_2O concentration onto its own lifetime following Meinshausen et al. (2011b).

$$\tau = \tau_o \left(\frac{C}{C_o}\right)^{-0.05} \tag{B11}$$

where τ_o and C_o are reference state values. In Eq. (B11) we use present-day numbers for the reference state (instead of preindustrial values) of $C_o = 316\,ppbv$ (Meinshausen et al., 2011a) and $\tau_o = 114\,yr$ (Forster et al., 2007). Using emissions data from the Meinshausen et al. (2011a) RCP4.5 time series, we ran the box model to a steady state N_2O concentration ($dC/dt = 0$) for 1850, 2000, and 2100 anthropogenic and natural N_2O emissions. We assume N_2O uptake by the soil is accounted for in the emissions term and doesn't affect the atmospheric lifetime.

After these simulations that include all emissions, the emissions from fires are removed and the model is run to a new steady state. Due to the long lifetime of N_2O in the atmosphere, the simulation can take several hundred model years to reach equilibrium after the emissions perturbation. The following expression from Ramaswamy et al. (2001) is used to compute the RF of the perturbed N_2O concentration:

$$\Delta F = 0.12\left(\sqrt{N} - \sqrt{N_o}\right) - \left[f\left(M_o, N\right) - f\left(M_o, N_o\right)\right] \tag{B12}$$

ACPD
12, 10535–10621, 2012

B5 Aerosol direct and indirect effects

Particle emissions from fires contain mainly carbonaceous material with minor contributions from dust and inorganic salts such as sulfate and nitrate. Globally, biomass burning is thought to be the largest source of primary organic carbon and black carbon aerosols (Mahowald et al., 2011b). Aerosols scatter solar radiation, a cooling effect, but some aerosol species, notably black carbon, absorb solar radiation and warm the troposphere. Fires emit a combination of scattering and absorbing aerosols leading to partially canceling radiative effects. The direct effect further depends on the albedo of the underlying surface, which can include clouds. The cloud fraction and cloud heights are particularly important over the ocean where they introduce a highly reflective surface over a strong absorbing surface. Sakaeda et al. (2011) note that the direct effect of biomass burning aerosols off the western coast of Africa is controlled in large part by the extent of the stratocumulus deck in this region.

To compute the direct effect of fire aerosols in this study we ran online radiation diagnostics during the AERO group of simulations for which radiative fluxes are calculated including all aerosols and again with the radiative impacts of aerosols removed. The direct effect RF is defined here as the difference in the change in TOA shortwave flux due to aerosol scattering and absorption (the two processes removed during the online diagnostics) that arises from the different emissions (fire against no-fire). This forcing is assessed for all-sky and clear-sky conditions.

Aerosols also impact radiative transfer indirectly by their effects on clouds. Acting as nuclei for cloud droplets and ice crystals, aerosols affect the sizes of the cloud particles leading to changes in the cloud albedo, know as the first indirect aerosol effect. Lohmann and Feichter (2005) list several other important indirect effects of aerosols including impacts on cloud lifetime and feedbacks onto mixed-phase clouds. Moreover, absorbing aerosols add heat to the atmosphere and change the vertical temperature profile, affecting the cloud cover and cloud liquid water path. This is known as the semi-direct effect since it occurs as a result of the direct effect (Lohmann and Feichter, 2005).

ACPD
12, 10535–10621, 2012

Sakaeda et al. (2011) found a semi-direct effect from fire aerosols emitted over Central Africa that was of similar magnitude to the direct effect in the same region. In their study, the semi-direct effect was strongly negative over ocean clouds, which increased in coverage with the increased aerosols, and positive over land for which clouds did not increase in coverage but decreased in liquid water content.

We define the indirect effect of fire aerosols as the change in total cloud forcing (TCF) between the fire and no-fire aerosol simulations, where TCF = shortwave cloud forcing (SWCF) + longwave cloud forcing (LWCF). The TCF is assessed at the TOA after removing direct interaction between aerosols and radiation using the online radiation diagnostics. The shortwave portion of this quantity is roughly equivalent to the residual aerosol forcing after the direct effect has been removed. In other words, the indirect effects can be defined here as the total shortwave aerosol forcing minus the direct effect, and finally, with longwave cloud forcing added in. This definition is not equivalent to the indirect effect as defined by the IPCC because it includes indirect effects in addition to the cloud albedo effect, such as the cloud lifetime effect, and the semi-direct effect of absorbing aerosols. It is in this sense, however, representative of the total impact of fire aerosols.

The aerosol effects can be expressed by three simple relationships for shortwave forcing:

$$\text{TOTAL AEROSOL EFFECT} = \Delta\left(\text{FSNT}_\text{A}\right) \tag{B13}$$

$$\text{DIRECT AEROSOL EFFECT} = \Delta\left(\text{FSNT}_\text{A} - \text{FSNT}_\text{N}\right) \tag{B14}$$

$$\text{INDIRECT AEROSOL EFFECTS}\left(\text{Shortwave}\right) = \Delta\left(\text{FSNT}_\text{N}\right) \approx \Delta(\text{SWCF}_\text{N}) \tag{B15}$$

Here FSNT stands for the net TOA shortwave flux, Δ represents the difference in the radiative flux expression between the simulation with fire aerosols and the simulation without fire aerosols, and the subscripts indicate the flux was diagnosed with direct aerosol effects, A, and without direct aerosol effects, N.

ACPD
12, 10535–10621, 2012

B6 Land albedo changes

Trajectories of post-fire land surface albedo based on the literature were used for our analyses (Fig. B2). These are necessarily over-simplifications of complex pyrogenic, ecological, and land use processes. They are designed only to represent broad-scale patterns of albedo through time for the major fire-affected ecosystems on Earth, and provide bounds for landscape impacts on the global energy budget in the context of other fire effects. We do not consider the impact of fires on the interdependence of atmospheric aerosol RF and surface albedo RF changes (Betts et al., 2007).

The first panel (Fig. B2a) shows relatively quick recoveries representative of tropical grasslands and savannas. Because rain removes black carbon and stimulates grass growth, these recovery rates depend on the seasonal timing of fire (Fisch et al., 1994; Beringer et al., 2003). While savanna albedos recover relatively quickly (within a year or two, depending on tree density and canopy scorch), long-term woody encroachment can occur within a couple decades in the absence of fire and cause a slight decrease in albedo (Brookman-Amissah et al., 1980; Higgins et al., 2007). This effect is shown in Fig. B2b but was not included in our RF estimate. Globally, there is a wide range of pre-fire grassland and savanna albedos. Underlying soil color also varies substantially, and can influence the magnitude and sign of post-fire albedo changes (Fisch et al., 1994). For this analysis we assume that extratropical grasses and crops follow the same albedo recovery period as tropical grasses, regardless of season. We also use a similar recovery curve for boreal shrubs but extend the recovery period to three years, based on work by Veraverbeke et al. (2011).

Tropical forest fires cause increased albedos because of the emergence of secondary vegetation (Giambelluca et al., 1997). If not converted to agriculture or pasture, the landscape albedo recovers within a decade, even though mature trees and climax species have not yet been established. The last panel (Fig. B2c) represents albedo change from boreal forest fires in North America. After an initial decrease, sum-

ACPD
12, 10535–10621, 2012

mer albedo is increased for many decades because of a mid-successional deciduous phase. Winter and spring albedo is increased dramatically because of snow exposure.

The curves given in Fig. B2 are applied to our model estimates of area burned and surface albedo using the following method. First, we compute the monthly mean surface albedos as the ratio of outgoing to incoming surface shortwave radiation at each model grid point, predicted by CAM5 in the AERO group of simulations that did not include fire emissions. It should be noted that the monthly values are averaged over the five years of these simulations. Next we find the fraction of shortwave radiation leaving the surface that makes it back to the TOA (TOA_frac). Using the computed albedos as the initial values for each point, we apply the albedo curves to the CLM3 or GFEDv2 fractional area burned and fractional PFTs (in each case using the time period specific databases) in each grid box. Tropical savanna was defined in PFT terms as 70 % warm C4 grass and 30 % tropical evergreen broadleaf tree with the proportions based on those used by Bonan et al. (2002). In gridcells dominated by C4 grasses any fraction not considered savanna was accounted for as grassland. The winter albedo recovery curve was applied wherever monthly average snow depth water equivalent exceeded 1 cm.

The change in albedo will act to increase or decrease the outgoing shortwave radiation from the surface. This is multiplied by the TOA_frac, so that RF scales linearly with the outgoing surface shortwave radiation. This analysis is carried out on monthly, rather than annual, means so that the seasonal differences in albedo changes are accounted for. The impacts of the albedo changes on the radiation balance are computed for 100 yr, after which all biomes have recovered and returned to their initial albedo.

Acknowledgements. We would like to thank Maria val Martin of Colorado State University for her assistance and acknowledge funding from the National Science Foundation (NSF AGS-0758369). Model integrations were performed with a National Center for Atmospheric Research facility, which is sponsored by the NSF.

ACPD
12, 10535–10621, 2012

References

Akagi, S. K., Yokelson, R. J., Wiedinmyer, C., Alvarado, M. J., Reid, J. S., Karl, T., Crounse, J. D., and Wennberg, P. O.: Emission factors for open and domestic biomass burning for use in atmospheric models, Atmos. Chem. Phys., 11, 4039–4072, doi:10.5194/acp-11-4039-2011, 2011.

Amiro, B. D., Orchansky, A. L., Barr, A. G., Black, T. A., Chambers, S. D., Chapin III, F. S., Goulden, M. L., Litvak, M., Liu, H. P., and McCaughey, J. H.: The effect of post-fire stand age on the boreal forest energy balance, Agr. Forest Meteorol., 140, 41–50, doi:10.1016/j.agrformet.2006.02.014, 2006.

Andreae, M. O. and Merlet, P.: Emission of trace gases and aerosols from biomass burning, Global Biogeochem. Cy., 15, 955–966, 2001.

Andreae, M. O. and Rosenfeld, D.: Aerosol–cloud–precipitation interactions, Part 1: the nature and sources of cloud-active aerosols, Earth-Sci. Rev., 89, 955–966, doi:10.1016/j.earscirev.2008.03.001, 2008.

Archer, D., Eby, M., Brovkin, V., Ridgwell, A., Cao, L., Mikolajewicz, U., Cladeira, K., Matsumoto, K., Munhoven, G., Montenegro, A., and Tokos, K.: Atmospheric lifetime of fossil fuel carbon dioxide, Annu. Rev. Earth Pl. Sc., 37, 117–134, doi:10.1146/annurev.earth.031208.100206, 2009.

Arora, V. K. and Boer, G. J.: Fire as an interactive component of dynamic vegetation models, J. Geophys. Res., 110, G02008, doi:10.1029/2005JG000042, 2005.

Beringer, J., Hutley, L. B., Tapper, N. J., Kerley, A., Coutts, A., and O'Grady, A. P.: Fire impacts on surface heat, moisture and carbon fluxes from a tropical savanna in Northern Australia, Int. J. Wildland Fire, 12, 333–340, doi:10.1071/WF03023, 2003.

Betts, R. A., Falloon, P. D., Goldewijk, K. K., and Ramankutty, N.: Biogeophysical effects of land use on climate: model simulations of radiative forcing and large-scale temperature change, Agr. Forest Meteorol., 142, 216–233, doi:10.1016/j.agrformet.2006.08.021, 2007.

Bian, H., Chin, M., Kawa, S. R., Duncan, B., Arellano, A., and Kasibhatla, P.: Sensitivity of global CO simulations to uncertainties in biomass burning sources, J. Geophys. Res., 112, D23308, doi:10.1029/2006JD008376, 2007.

Bonan, G. B., Oleson, K. W., Vertenstein, M., Levis, S., Zeng, X. B., Dai, Y. J., Dickinson, R. E., and Yang, Z. L.: The land surface climatology of the community land model coupled to the NCAR community climate model, J. Climate, 15, 3123–3149, doi:10.1175/1520-0442, 2002.

ACPD
12, 10535–10621, 2012

Bond, W. J., Woodward, F. I., and Midgley, G. F.: The global distribution of ecosystems in a world without fire, New Phytol., 165, 525–538, doi:10.1111/j.1469-8137.2004.01252.x, 2005.

Bowman, D. M. J. S., Balch, J. K., Artaxo, P., Bond, W. J., Carlson, J. M., Cochrane, M. A., D'Antonio, C. M., DeFries, R., Doyle, J. C., Harrison, S. P., Johnston, F. H., Keeley, J. E., Krawchuk, M. A., Kull, C. A., Marston, J. B., Mortiz, M. A., Prentice, I. C., Roos, C. I., Scott, A. C., Swetnam, T. W., van der Werf, G. R., and Pyne, S. J.: Fire in the earth system, Science, 324, 481, doi:10.1126/science.1163886, 2009.

Brookman-Amissah, J., Hall, J. B., Swaine, M. D., and Attakorah, J. Y.: A re-assessment of a fire protection experiment in North-Eastern Ghana savanna, J. Appl. Ecol., 17, 85–99, doi:10.2307/2402965, 1980.

Carslaw, K. S., Boucher, O., Spracklen, D. V., Mann, G. W., Rae, J. G. L., Woodward, S., and Kulmala, M.: A review of natural aerosol interactions and feedbacks within the Earth system, Atmos. Chem. Phys., 10, 1701–1737, doi:10.5194/acp-10-1701-2010, 2010.

Chen, Y., Randerson, J., van der Werf, G., Morton, D., Mu, M., and Kasibhatla, P.: Nitrogen deposition in tropical forests from savanna and deforestation fires, Glob. Change Biol., 16, 2024–2038, 2010.

Mian Chin, Diehl, T., Dubovik, O., Eck, T. F., Holben, B. N., Sinyuk, A., and Streets, D. G.: Light absorption by pollution, dust, and biomass burning aerosols: a global model study and evaluation with AERONET measurements, Ann. Geophys., 27, 3439–3464, doi:10.5194/angeo-27-3439-2009, 2009.

Chuang, C. C., Penner, J. E., Prospero, J. M., Grant, K. E., Rau, G. H., Kawamoto, K.: Cloud susceptibility and the first aerosol indirect forcing: sensitivity to black carbon and aerosol concentrations, J. Geophys. Res., 107(D21), 4564, doi:10.1029/2000JD000215, 2002.

Cofer, W. R., Levine, J. S., Winstead, E. L., and Stocks, B. J.: New estimates of nitrous oxide emissions from biomass burning, Nature, 349, 689–691, 1991.

Crutzen, P. J. and Andreae, M. O.: Biomass burning in the tropics: impact on atmospheric chemistry and biogeochemical cycles, Science, 250, 1669–1678, 1990.

Culf, A. D., Fisch, G., and Hodnett, M. G.: The albedo of Amazonian forest and ranch land, J. Climate, 8, 1544–1554, doi:10.1175/1520-0442, 1995.

Decker, R. M. and Zeng, X.: Impact of modified richards equation on global soil moisture simulation in the Community Land Model (CLM3.5), J. Adv. Model. Earth Syst., 1, 22 pp., doi:10.3894/JAME S.2009.1.5, 2009.

ACPD
12, 10535–10621, 2012

Dentener, F., Stevenson, D., Cofala, J., Mechler, R., Amann, M., Bergamaschi, P., Raes, F., and Derwent, R.: The impact of air pollutant and methane emission controls on tropospheric ozone and radiative forcing: CTM calculations for the period 1990–2030, Atmos. Chem. Phys., 5, 1731–1755, doi:10.5194/acp-5-1731-2005, 2005.

Emmons, L. K., Walters, S., Hess, P. G., Lamarque, J.-F., Pfister, G. G., Fillmore, D., Granier, C., Guenther, A., Kinnison, D., Laepple, T., Orlando, J., Tie, X., Tyndall, G., Wiedinmyer, C., Baughcum, S. L., and Kloster, S.: Description and evaluation of the Model for Ozone and Related chemical Tracers, version 4 (MOZART-4), Geosci. Model Dev., 3, 43–67, 2010.

Enting, I., Wigley, T. M. L., and Heimann, M.: Future Emissions and Concentrations of Carbon Dioxide: Key Ocean/Atmosphere/Land Analyses, Technical Paper, CSIRO Division of Atmospheric Research, Australia, 31, 1994.

Fiore, A. M., Dentener, F. J., Wild, O., Cuvelier, C., Schultz, M. G., Hess, P., Textor, C., Schulz, M., Doherty, R. M., Horowitz, L. W., MacKenzie, I. A., Sanderson, M. G., Shindell, D. T., Stevenson, D. S., Szopa, S., Van Dingenen, R., Zeng, G., Atherton, C., Bergmann, D., Bey, I., Carmichael, G., Collins, W. J., Duncan, B. N., Faluvegi, G., Folberth, G., Gauss, M., Gong, S., Hauglustaine, D., Holloway, T., Isaksen, I. S. A., Jacob, D. J., Jonson, J. E., Kaminski, J. W., Keating, T. J., Lupu, A., Marmer, E., Montanaro, V., Park, R. J., Pitari, G., Pringle, K. J., Pyle, J. A., Schroeder, S., Vivanco, M. G., Wind, P., Wojcik, G., Wu, S., and Zuber, A.: Multimodel estimates of intercontinental source-receptor relationships for ozone pollution, J. Geophys. Res., 114, D04301, doi:10.1029/2008jd010816, 2009.

Fisch, G., Wright, I. R., and Bastable, H. G.: Albedo of tropical grass: a case study of pre and post burning, Int. J. Climatol., 14, 103–107, doi:10.1002/joc.3370140109, 1994.

Flanner, M. G. and Zender, C. S.: Snowpack radiative heating: influence on Tibetan Plateau climate, J. Geophys. Res., 32, L06501, doi:10.1029/2004GL022076, 2005.

Flanner, M. G. and Zender, C. S.: Linking snowpack microphysics and albedo evolution, J. Geophys. Res., 111, D12208, doi:10.1029/2005JD006834, 2006.

Flanner, M. G., Zender, C. S., Randerson, J. T., and Rasch, P. J.: Present-day climate forcing and response from black carbon in snow, J. Geophys. Res., 112, D11202, doi:10.1029/2006JD008003, 2007.

Flanner, M. G., Zender, C. S., Hess, P. G., Mahowald, N. M., Painter, T. H., Ramanathan, V., and Rasch, P. J.: Springtime warming and reduced snow cover from carbonaceous particles, Atmos. Chem. Phys., 9, 2481–2497, doi:10.5194/acp-9-2481-2009, 2009.

ACPD
12, 10535–10621, 2012

Forster, P., Ramaswamy, V., Artaxo, P., Berntsen, T., Betts, R., Fahey, D. W., Haywood, J., Lean, J., Lowe, D. C., Myhre, G., Nganga, J., Prinn, R., Raga, G., Schulz, M., and Dorland, R. V.: Changes in Atmospheric Constituents and in Radiative Forcing, in: Climate Change 2007: The Physical Science Basis. Contribution of Working Group I to the Fourth Assessment Report of the Intergovernmental Panel on Climate Change, edited by: Solomon, S., Qin, D., Manning, M., Chen, Z., Marquis, M., Averyt, K. B., Tignor, M., and Miller, H. L., Cambridge University Press, Cambridge and New York, 2007.

Friedlingstein, P. and Prentice, I. C.: Carbon-climate feedbacks: a review of model and observation based estimates, Curr. Opin. Environ. Sustain., 2, 251–257, 2010.

Friedlingstein, P., Cox, P., Betts, R., Bopp, L., von Bloh, W., Brovkin, V., Cadule, P., Doney, S., Eby, M., Fung, I., Bala, G., John, J., Jones, C., Joos, F., Kato, T., Kawamiya, M., Knorr, W., Lindsay, K., Matthews, H. D., Raddatz, T., Rayner, P., Reick, C., Roeckner, E., Schnitzler, K.-G., Schnur, R., Strassmann, K., Weaver, A. J., Yoshikawa, C., and Zeng, N.: Climate-carbon cycle feedback analysis, results from the C4MIP model intercomparison, J. Climate, 19, 3337–3353, 2006.

Fuglestvedt, J. S., Bernsten, T. K., Isaksen, I. S. A., Mao, H., Liang, X.-Z., and Wang, W.-C.: Climatic forcing of nitrogen oxides through changes in tropospheric ozone and methane; global 3D model studies, Atmos. Environ., 33, 961–977, 1999.

Fuller, D. O. and Ottke, C.: Land cover, rainfall and land-surface albedo in West Africa, Climatic Change, 54, 181–204, doi:10.1023/A:1015730900622, 2002.

Galanter, M., Levy, H., and Carmichael, G. R.: Impacts of biomass burning on tropospheric CO, NO_x, and O_3, J. Geophys. Res.-Atmos., 105, 6633–6653, 2000.

Gettelman, A., Liu, X., Ghan, S. J., Morrison, H., Park, S., Conley, A. J., Klein, S. A., Boyle, J., Mitchell, D. L., and Li, J. L. F.: Global simulations of ice nucleation and ice supersaturation with an improved cloud scheme in the Community Atmosphere Model, J. Geophys. Res.-Atmos., 115, D18216, doi:10.1029/2009jd013797, 2010.

Gettelman, A., Kay, J. E., and Shell, K. M.: The evolution of climate sensitivity and climate feedbacks in the Community Atmosphere Model, J. Climate, 25, 1454–1469, doi:10.1175/JCLI-D-11-00197.1, 2012.

Giambelluca, T. W., Hölscher, D., Bastos, T. X., Frazão, R. R., Nullet, M. A., and Ziegler, A. D.: Observations of albedo and radiation balance over postforest land surfaces in the Eastern Amazon Basin, J. Climate, 10, 919–928, doi:10.1175/1520-0442, 1997.

ACPD
12, 10535–10621, 2012

Goodwin, P., Williams, R. G., Follows, M. J., and Dutkiewicz, S.: Ocean-atmosphere partitioning of anthropogenic carbon dioxide on centennial timescales, Global Biogeochem. Cy., 21, GB1014, doi:10.1029/2006GB002810, 2007.

Govaerts, Y. M., Pereira, J. M., Pinty, B., and Mota, B.: Impact of fires on surface albedo dynamics over the African continent, J. Geophys. Res.-Atmos., 107(D22), 4629, doi:10.1029/2002JD002388, 2002.

Granier, C., Muller, J.-F., and Brasseur, G.: The impact of biomass burning on the global budget of ozone and ozone precursors, in: Biomass Burning and its Interrelationship with the Climate System, Innes, J. L., Beniston, M., and Verstraete, M. M. (eds.), 69–85, Kluwer Acad., Norwell, MA, 2000.

Guieu, C., Bonnet, S., Wagener, T., and Loye-Pilot, M.-D.: Biomass burning as a source of dissolved iron to the open ocean? Geophys. Res. Lett., 22, L19608, doi:10.1029/12005GL022962, 2005.

Hadley, O. L., Corrigan, C. E., Kirchstetter, T. W., Cliff, S. S., and Ramanathan, V.: Measured black carbon deposition on the Sierra Nevada snow pack and implication for snow pack retreat, Atmos. Chem. Phys., 10, 7505–7513, doi:10.5194/acp-10-7505-2010, 2010.

Hansen, J., Sato, M., Ruedy, R., Nazarenko, L., Lacis, A., Schmidt, G. A., Russell, G., Aleinov, I., Bauer, M., Bauer, S., Bell, N., Cairns, B., Canuto, V., Chandler, M., Cheng, Y., Del Genio, A., Faluvegi, G., Fleming, E., Friend, A., Hall, T., Jackman, C., Kelley, M., Kiang, N., Koch, D., Lean, J., Lerner, J., Lo, K., Menon, S., Miller, R., Minnis, P., Novakov, T., Oinas, V., Perlwitz, Ja., Perlwitz, Ju., Rind, D., Romanou, A., Shindell, D., Stone, P., Sun, S., Tausnev, N., Thresher, D., Wielicki, B., Wong, T., Yao, M., and Zhang, S.: Efficacy of climate forcings, J. Geophys. Res.-Atmos., 110, D18104, doi:10.1029/2005JD005776, 2005.

Hanson, H. P.: Marine stratocumulus climatologies, Int. J. Climatol., 11, 147–164, 1991.

Harrison, S. P., Marlon, J. R., and Bartlein, P. J.: Fire in the earth system, in: Changing Climates, Earth Systems and Society, International Year of Planet Earth, Dodson, J. (ed.), Springer, New York, USA, 2010.

van den Heever, S. C., Stephens, G. L., and Wood, N. B.: Aerosol indirect effects on tropical convection characteristics under conditions of radiative-convective equilibrium, J. Atmos. Sci., 68, 699–717, doi:10.1175/2010jas3603.1, 2011.

Higgins, S. I., Bond, W. J., February, E. C., Bronn, A., Euston-Brown, D. I. W., Enslin, B., Govender, N., Rademan, L., O'Regan, S., Potgieter, A. L. F., Scheiter, S., Sowry, R., Trollope, L.,

ACPD
12, 10535–10621, 2012

and Trollope, W. S. W.: Effects of four decades of fire manipulation on woody vegetation structure in savanna, Ecology, 88, 1119–1125, doi:10.1890/06-1664, 2007.
Hoelzemann, J. J., Schultz, M. G., Brasseur, G. P., Granier, C., and Simon, M.: Global Wildland Fire Emission Model (GWEM): evaluating the use of global area burnt satellite data, J. Geophys. Res., 109, D14S04, doi:10.1029/2003JD003666, 2004.
Hurtt, G. C., Frolking, S., Fearon, M. G., Moore, B., Shevliakova, E., Malyshev, S., Pacala, S. W., and Houghton, R. A.: The underpinnings of land-use history: three centuries of global gridded land-use transitions, wood-harvest activity, and resulting secondary lands, Glob. Change Biol., 12, 1208–1229, doi:10.1111/j.1365-2486.2006.01150.x, 2006.
Hyer, E. J., Reid, J. S., and Zhang, J.: An over-land aerosol optical depth data set for data assimilation by filtering, correction, and aggregation of MODIS Collection 5 optical depth retrievals, Atmos. Meas. Tech., 4, 379–408, doi:10.5194/amt-4-379-2011, 2011.
Ito, A., Sudo, K., Akimoto, H., Sillman, S., and Penner, J. E.: Global modeling analysis of tropospheric ozone and its radiative forcing from biomass burning emissions in the twentieth century, J. Geophys. Res.-Atmos., 112, D24307, doi:10.1029/2007JD008745, 2007.
Jacobson, M. Z.: The short-term cooling but long-term global warming due to biomass burning, J. Climate, 17, 2909–2926, 2004.
Jin, Y. and Roy, D. P.: Fire-induced albedo change and its radiative forcing at the surface in Northern Australia, Geophys. Res. Lett., 32, L13401, doi:10.1029/2005GL022822, 2005.
Johnston, F. H., Henderson, S. B., Chen, Y., Randerson, J. R., Marlier, M., DeFries, R. S., Kinney, P., Bowman, D. M., and Brauer, M.: Estimated global mortality attributable to smoke from landscape fires, Environ. Health Persp., doi:10.1289/ehp.1104422, 2012.
Jones, A., Roberts, D. L., Woodage, M., and Johnson, C.: Indirect sulphate aerosol forcing in a climate model with an interactive sulphur cycle, J. Geophys. Res.-Atmos., 106, 20293–20310, 2001.
Kahn, R. A., Gaitley, B. J., Martonchik, J. V., Diner, D. V., and Crean, K. A.: Multiangle Imaging Spectroradiometer (MISR) global aerosol optical depth validation based on 2 years of coincident Aerosol Robotic Network (AERONET) observations, J. Geophys. Res.-Atmos., 110, D10S04, doi:10.1029/2004JD004706, 2005.
Kloster, S., Mahowald, N. M., Randerson, J. T., Thornton, P. E., Hoffman, F. M., Levis, S., Lawrence, P. J., Feddema, J. J., Oleson, K. W., and Lawrence, D. M.: Fire dynamics during the 20th century simulated by the Community Land Model, Biogeosciences, 7, 1877–1902, doi:10.5194/bg-7-1877-2010, 2010.

ACPD
12, 10535–10621, 2012

Kloster, S., Mahowald, N. M., Randerson, J. T., and Lawrence, P. J.: The impacts of climate, land use, and demography on fires during the 21st century simulated by CLM-CN, Biogeosciences, 9, 509–525, doi:10.5194/bg-9-509-2012, 2012.

Knorr, W.: Is the airborne fraction of anthropogenic CO_2 emissions increasing? Geophys. Res. Lett., 36, L21710, doi:10.1029/2009GL040613, 2009.

Koch, D., Schulz, M., Kinne, S., McNaughton, C., Spackman, J. R., Balkanski, Y., Bauer, S., Berntsen, T., Bond, T. C., Boucher, O., Chin, M., Clarke, A., De Luca, N., Dentener, F., Diehl, T., Dubovik, O., Easter, R., Fahey, D. W., Feichter, J., Fillmore, D., Freitag, S., Ghan, S., Ginoux, P., Gong, S., Horowitz, L., Iversen, T., Kirkevåg, A., Klimont, Z., Kondo, Y., Krol, M., Liu, X., Miller, R., Montanaro, V., Moteki, N., Myhre, G., Penner, J. E., Perlwitz, J., Pitari, G., Reddy, S., Sahu, L., Sakamoto, H., Schuster, G., Schwarz, J. P., Seland, Ø., Stier, P., Takegawa, N., Takemura, T., Textor, C., van Aardenne, J. A., and Zhao, Y.: Evaluation of black carbon estimations in global aerosol models, Atmos. Chem. Phys., 9, 9001–9026, doi:10.5194/acp-9-9001-2009, 2009.

Krishnamurthy, A., Moore, J. K., Mahowald, N., Luo, C., Doney, S. C., Lindsay, K., and Zender, C. S.: Impacts of increasing anthropogenic soluble iron and nitrogen deposition on ocean biogeochemistry, Global Biogeochem. Cy., 23, GB3016, doi:10.1029/2008GB003440, 2009.

Krishnamurthy, A., Moore, J. K., Mahowald, N., Luo, C., Zender, C. S.: Impacts of atmospheric nutrient inputs on marine biogeochemistry, J. Geophys. Res.-Biogeo., 115, G01006, doi:10.1029/2009JG001115, 2010.

Kroeze, C., Mosier, A., and Bouwman, L.: Closing the global N_2O budget: a retrospective analysis 1500–1994, Global Biogeochem. Cy., 13, 1–8, 1999.

Lamarque, J.-F., Kiehl, J., Brasseur, G., Butler, T., Cameron-Smith, P., Collins, W. D., Collins, W. J., Granier, C., Hauglustaine, D., Hess, P., Holland, E., Horowitz, L., Lawrence, M., McKenna, D., Merilees, P., Prather, M., Rasch, P., Rotman, D., Shindell, D., and Thornton, P.: Assessing future nitrogen deposition and carbon cycle feedbacks using a multi-model approach: analysis of nitrogen deposition, J. Geophys. Res., 110, D19303, doi:10.1029/2005JD005825, 2005.

Lamarque, J.-F., Bond, T. C., Eyring, V., Granier, C., Heil, A., Klimont, Z., Lee, D., Liousse, C., Mieville, A., Owen, B., Schultz, M. G., Shindell, D., Smith, S. J., Stehfest, E., Van Aardenne, J., Cooper, O. R., Kainuma, M., Mahowald, N., McConnell, J. R., Naik, V., Riahi, K., and van Vuuren, D. P.: Historical (1850–2000) gridded anthropogenic and biomass burn-

ACPD
12, 10535–10621, 2012

ing emissions of reactive gases and aerosols: methodology and application, Atmos. Chem. Phys., 10, 7017–7039, doi:10.5194/acp-10-7017-2010, 2010.
Lamarque, J.-F., Emmons, L. K., Hess, P. G., Kinnison, D. E., Tilmes, S., Vitt, F., Heald, C. L., Holland, E. A., Lauritzen, P. H., Neu, J., Orlando, J. J., Rasch, P., and Tyndall, G.: CAM-chem: description and evaluation of interactive atmospheric chemistry in CESM, Geosci. Model Dev. Discuss., 4, 2199–2278, doi:10.5194/gmdd-4-2199-2011, 2011.
Lawrence, D. M. and Slater, A. G.: Incoporating organic soil into a global climate model, Clim. Dynam., 30, 2–3, doi:10.1007/s00382-007-0278-1, 2008.
Lawrence, D. M. and Slater, A. G.: The contribution of snow condition trends to future ground climate, Clim. Dynam., 34, 7–8, doi:10.1007/s00382-009-0537-4, 2009.
Lawrence, D. M., Oleson, K. W., Flanner, M. G., Thornton, P. E., Swenson, S. C., Lawrence, P. J., Zeng, X., Yang, Z.-L., Levis, S., Sakaguchi, K., Bonan, G. B., and Slater, A. G.: Parameterization improvements and functional and structural advances in Version 4 of the Community Land Model, J. Adv. Model. Earth Syst., 3, 1–27, doi:10.1029/2011MS000045, 2011.
Liu, H., Randerson, J. T., Lindfors, J., and Chapin, F. S.: Changes in the surface energy budget after fire in boreal ecosystems of interior Alaska: an annual perspective, J. Geophys. Res.-Atmos., 10, D13101, doi:10.1029/2004JD005158, 2005.
Liu, X., Easter, R. C., Ghan, S. J., Zaveri, R., Rasch, P., Shi, X., Lamarque, J.-F., Gettelman, A., Morrison, H., Vitt, F., Conley, A., Park, S., Neale, R., Hannay, C., Ekman, A. M. L., Hess, P., Mahowald, N., Collins, W., Iacono, M. J., Bretherton, C. S., Flanner, M. G., and Mitchell, D.: Toward a minimal representation of aerosol direct and indirect effects: model description and evaluation, Geosci. Model Dev. Discuss., 4, 3485–3598, doi:10.5194/gmdd-4-3485-2011, 2011a.
Liu, X., Xie, S., Boyle, J., Klein, S. A., Shi, X., Wang, Z., Lin, W., Ghan, S. J., Earle, M., Liu, P. S. K., and Zelenyuk, A.: Testing cloud microphysics parameterizations in NCAR CAM5 with ISDAC and M-PACE observations, J. Geophys. Res.-Atmos., 116, D00T11, doi:10.1029/2011JD015889, 2011b.
Lohmann, U. and Feichter, J.: Global indirect aerosol effects: a review, Atmos. Chem. Phys., 5, 715–737, doi:10.5194/acp-5-715-2005, 2005.
Longo, K. M., Freitas, S. R., Andreae, M. O., Yokelson, R., and Artaxo, P.: Biomass burning in Amazonia: emissions, long-range transport of smoke and its regional and remote impacts, Geoph. Monog. Series, 186, 207–232, doi:10.1029/2008GM000847, 2009.

ACPD
12, 10535–10621, 2012

Lyons, E. A., Jin, Y., Randerson, J. T., and Hall, C.: Changes in surface albedo after fire in boreal forest ecosystems of interior Alaska assessed using MODIS satellite observations, J. Geophys. Res.-Biogeo., 113, G02012, doi:10.1029/2007JG000606, 2008.

Mahowald, N.: Aerosol indirect effect on biogeochemistry and climate, Science, 334, 794–796, 2011.

Mahowald, N., Artaxo, P., Baker, A., Jickells, T., Okin, G., Randerson, J., and Townsend, A.: Impact of biomass burning emissions and land use change on Amazonian atmospheric cycling and deposition of phosphorus, Global Biogeochem. Cy., 19, GB4030, doi:10.1029/2005GB002541, 2005.

Mahowald, N., Lindsay, K., Rothenberg, D., Doney, S. C., Moore, J. K., Thornton, P., Randerson, J. T., and Jones, C. D.: Desert dust and anthropogenic aerosol interactions in the Community Climate System Model coupled-carbon-climate model, Biogeosciences, 8, 387–414, doi:10.5194/bg-8-387-2011, 2011a.

Mahowald, N. M., Ward, D. S., Kloster, S., Flanner, M. G., Heald, C. L., Heavens, N. G., Hess, P. G., Lamarque, J.-F., and Chuang, P. Y.: Aerosol impacts on climate and biogeochemistry, Annu. Rev. Env. Resour., 36, 45–74, doi:10.1146/annurev-environ-042009-094507, 2011b.

Mao, Y. H., Li, Q. B., Zhang, L., Chen, Y., Randerson, J. T., Chen, D., and Liou, K. N.: Biomass burning contribution to black carbon in the Western United States Mountain Ranges, Atmos. Chem. Phys., 11, 11253–11266, doi:10.5194/acp-11-11253-2011, 2011.

Marlon, J. R., Bartlein, P. J., Carcaillet, C., Gavin, D. G., Higuera, P. E., Joos, F., Power, M. J., and Prentice, I. C.: Climate and human influences on global biomass burning over the past two millennia, Nature Geosci., 1, 697–702, doi:10.1038/ngeo313, 2008.

Martin, J., Gordon, R. M., and Fitzwater, S. E.: The case for iron, Limnol. Oceanogr., 36, 1793–1802, 1991.

Matichuk, R. I., Colarco, P. R., Smith, J. A., and Toon, O. B.: Modeling the transport and optical properties of smoke aerosols from African savanna fires during the Southern African Regional Science Initiative campaign (SAFARI 2000), J. Geophys. Res., 112, D08203 doi:10.1029/2006JD007528, 2007.

Matichuk, R. I., Colarco, P. R., Smith, J. A., and Toon, O. B.: Modeling the transport and optical properties of smoke plumes from South American biomass burning, J. Geophys. Res.-Atmos., 113, D07208, doi:10.1029/2007JD009005, 2008.

ACPD
12, 10535–10621, 2012

McMillan, A., Winston, G. C., and Goulden, M. L.: Age dependent response of boreal forest to temperature and rainfall variability, Glob. Change Biol., 14, 1904–1916, doi:10.1111/j.1365-2486.2008.01614.x, 2008.

Meehl, G., Washington, W., Santer, B., Collins, W. D., Arblaster, J. M., Hu, A., Lawrence, D. M., Teng, H., Buja, L. E., and Strand, W. G.: Climate change projections for the twenty-first century and climate change commitment in the CCSM3, J. Climate, 19, 2597–2616, 2006.

Meinshausen, M., Smith, S. J., Calvin, K., Daniel, J. S., Kainuma, M. L. T., Lamarque, J- F., Matsumoto, K., Montzka, S. A., Raper, S. C. B., Riahi, K., Thomson, A., Velders, G. J. M., and van Vuuren, D. P. P.: The RCP greenhouse gas concentrations and their extensions from 1765 to 2300, Climatic Change, 109, 213–241, doi:10.1007/s10584-011-0156-z, 2011a.

Meinshausen, M., Raper, S. C. B., and Wigley, T. M. L.: Emulating coupled atmosphere-ocean and carbon cycle models with a simpler model, MAGICC6 – Part 1: Model description and calibration, Atmos. Chem. Phys., 11, 1417–1456, doi:10.5194/acp-11-1417-2011, 2011b.

Mieville, A., Granier, C., Liousse, C., Guillaume, B., Mouillot, F., Lamarque, J. F., Gregoire, J. M., and Petron, G.: Emissions of gases and particles from biomass burning during the 20th century using satellite data and a historical reconstruction, Atmos. Environ., 44(11), 1469–1477, doi:10.1016/j.atmosenv.2010.01.011, 2010.

Menon, S., Koch, D., Beig, G., Sahu, S., Fasullo, J., and Orlikowski, D.: Black carbon aerosols and the third polar ice cap, Atmos. Chem. Phys., 10, 4559–4571, doi:10.5194/acp-10-4559-2010, 2010.

Montzka, S. A., Fraser, P. J., Butler, J. H., Connell, P. S., Cunnold, D. M., Daniel, J. S., Derwent, R. G., Lal, S., McCulloch, A., Oram, D. E., Reeves, C. E., Sanhueza, E., Steele, L. P., Velders, G. J. M., Weiss, R. F., and Zander, R.: Controlled Substances and Other Source Gases, in Scientific Assessment of Ozone Depletion: 2002, Global Ozone Research and Monitoring Project, Report No. 47, chap. 1, 1.1–1.83, Global Ozone Resources and Monitoring Project, World Meteorol. Organ., Geneva, 2003.

Moss, R. H., Edmonds, J. A., Hibbard, K. A., Manning, M. R., Rose, S. K., van Vuuren, D. P., Carter, T. R., Emori, S., Kainuma, M., Kram, T., Meehl, G. A., Mitchell, J. F. B., Nakicenovix, N., Riahi, K., Smith, S. J., Stouer, R. J., Thomson, A. M., Weyant, J. P., and Wilbanks, T. J.: The next generation of scenarios for climate change research and assessment, Nature, 463, 747–56, doi:10.1038/nature08823, 2010.

ACPD
12, 10535–10621, 2012

Morrison, H. and Gettelman, A.: A new two-moment bulk stratiform cloud microphysics scheme in the community atmosphere model, version 3 (CAM3). Part I: description and numerical tests, J. Climate, 21, 3642–3659, doi:10.1175/2008jcli2105.1, 2008.

Myhre, G., Govaerts, Y., Haywood, J. M., Berntsen, T. K., and Lattanzio, A.: Radiative effect of surface albedo change from biomass burning, Geophys. Res. Lett, 32, L20812, doi:10.1029/2005GL022897, 2005.

Naik, V., Mauzerall, D., Horowitz, L., Schwarzkopf, M. D., Ramaswamy, V., and Oppenheimer, M.: Net radiative forcing due to changes in regional emissions of tropospheric ozone precursors, J. Geophys. Res.-Atmos., 110, D24306, doi:10.1029/2005JD005908, 2005.

Naik, V., Mauzerall, D., Horowitz, L., Schwarzkopf, M. D., Ramaswamy, V., and Oppenheimer, M.: On the sensitivity of radiative forcing from biomass burning aerosols and ozone to emission location, Geophys. Res. Lett., 34, L03818, doi:10.1029/2006GL028149, 2007.

Nakicenovic, N., Davidson, O., Davis, G., Gruebler, A., Kram, T., La Rovere, E. L., Metz, B., Morita, T., Pepper, W., Pitcher, H., Sankovski, A., Shukla, P., Swart, R., Watson, R., and Dadi, Z.: Special report on emissions scenarios, in: Contribution to the Intergovernmental Panel on Climate Change, Cambridge University Press, Cambridge, UK, 2000.

Nevison, C. D., Mahowald, N. M., Doney, S. C., Lima, I. D., van der Werf, G. R., Randerson, J. T., Baker, D. F., Kasibhatla, P., and McKinley, G. A.: Contribution of ocean, fossil fuel, land biosphere, and biomass burning carbon fluxes to seasonal and interannual variability in atmospheric CO_2, J. Geophys. Res.-Biogeo., 113, G01010, doi:10.1029/2007JG000408, 2008.

Niu, G.-Y. and Yang, Z.-L.: An observation-based formulation of snow cover fraction and its evaluation over large North American river basins, J. Geophys. Res.-Atmos., 112, D21101, doi:10.1029/2007JD008674, 2007.

Oleson, K. W., Niu, G.-Y., Yang, Z.-L., Lawrence, D. M., Thornton, P. E., Lawrence, P. J., Stoeckli, R., Dickinson, R. E., Bonan, G. B., Levis, S., Dai, A., and Qian, T.: Improvements to the Community Land Model and their impact on the hydrological cyle, J. Geophys. Res., 113, G01021, doi:10.1029/2007JG000563, 2008a.

Oleson, K. W., Bonan, G. B., Feddema, J., Vertenstein, M., and Grimmong, C. S. B.: An urban paramterization for a global climate model. 1. formulation and evaluation of two cities, J. Appl. Meteorol. Clim., 47, 1038–1060, 2008b.

Osborne, T. J. and Wigley, T. M. L.: A simple model for estimating methane concentration and lifetime variations, Clim. Dynam., 9, 181–193, 1994.

ACPD
12, 10535–10621, 2012

Pechony, O. and Shindell, D. T.: Driving forces of global wildfires over the past millennium and the forthcoming century, Proc. Natl. Acad. Sci., 107, 19167–19170, doi:10.1073/pnas.1003669107, 2010.
Pfister, G. G., Emmons, L. K., Hess, P. G., Honrath, R., Lamarque, J.-F., Val Martin, M., Owen, R. C., Avery, M. A., Browell, E. V., Holloway, J. S., Nedelec, P., Purvis, R., Ryerson, T. B., Sachse, G. W., and Schlager, H.: Ozone production from the 2004 North American boreal fires, J. Geophys. Res.-Atmos., 111, D24S07, doi:10.1029/2006JD007695, 2006.
Pfister, G. G., Wiedinmyer, C., and Emmons, L. K.: Impacts of the fall 2007 California wildfires on surface ozone: integrating local observations with global model simulations, Geophys. Res. Lett., 35, L19814, doi:10.1029/2008GL034747, 2008.
Pinker, R. T., Thompson, O. E., and Eck, T. F.: The albedo of a tropical evergreen forest, Q. J. Roy. Meteor. Soc., 106, 551–558, doi:10.1256/smsqj.44910, 1980.
Prather, M. J. and Hsu, J.: Coupling of nitrous oxide and methane by global atmospheric chemistry, Science, 330, 952–954, doi:10.1126/science.1196285, 2010.
Prather, M., Ehhalt, D., Dentener, F., Derwent, R., Dlugokencky, E., Holland, E., Isaksen, I., Katima, J., Kirchoff, V., Matson, P., Midgley, P., and Wang, M.: Atmospheric chemistry and greenhouse gases, in: Climate Change 2001, The scientific basis, Houghton, J. T., Ding, Y., Griggs, D. J., Noguer, M., Van der Linden, P. J., Dai, X., Maskell, K., and Johnson, C. A. (eds.), Intergovernmental Panel on Climate Change, Cambridge University Press, Cambridge, 239–287, 2001.
Prentice, I. C., Kelley, D. I., Foster, P. N., Friedlingstein, P., Harrison, S. P., and Bartlein, P. J.: Modeling fire and the terrestrial carbon balance, Glob. Biogeochem. Cy., 25, GB3005, doi:10.1029/2010GB003906, 2011.
Qian, T., Dai, A., Trenberth, K. E., and Oleson, K. W.: Simulation of global land surface conditions from 1948 to 2004. Part I: forcing data and evaluations, J. Hydrometeorol., 7, 953, doi:10.1175/JHM540.1, 2006.
Quaas, J., Ming, Y., Menon, S., Takemura, T., Wang, M., Penner, J. E., Gettelman, A., Lohmann, U., Bellouin, N., Boucher, O., Sayer, A. M., Thomas, G. E., McComiskey, A., Feingold, G., Hoose, C., Kristjánsson, J. E., Liu, X., Balkanski, Y., Donner, L. J., Ginoux, P. A., Stier, P., Grandey, B., Feichter, J., Sednev, I., Bauer, S. E., Koch, D., Grainger, R. G., Kirkevåg, A., Iversen, T., Seland, Ø., Easter, R., Ghan, S. J., Rasch, P. J., Morrison, H., Lamarque, J.-F., Iacono, M. J., Kinne, S., and Schulz, M.: Aerosol indirect effects – general

ACPD
12, 10535–10621, 2012

circulation model intercomparison and evaluation with satellite data, Atmos. Chem. Phys., 9, 8697–8717, doi:10.5194/acp-9-8697-2009, 2009.

Ramaswamy, V., Boucher, O., Haigh, J., Hauglustaine, D., Haywood, J., Myhre, G., Nakajima, T., Shi, G. Y., and Solomon, S.: Radiative forcing of climate change, in: Climate Change 2001, The Scientific Basis, Cambridge University Press, Cambridge, UK, 349–416, 2001.

Randerson, J. T., Liu, H., Flanner, M. G., Chambers, S. D., Jin, Y., Hess, P. G., Pfister, G., Mack, M. C., Treseder, K. K., Welp, L. R., Chapin, F. S., Harden, J. W., Goulden, M. L., Lyons, E., Ne, J. C., Schuur, E. A. G., and Zender, C. S.: The impact of boreal forest fire on climate warming, Science, 314, 1130–1132, doi:10.1126/science.1132075, 2006.

Real, E., Law, K. S., Weinzierl, B., Fiebig, M., Petzold, A., Wild, O., Methven, J., Arnold, S., Strohl, A., Huntrieser, H., Roiger, A., Schlager, H., Stewart, D., Avery, M., Sachse, G., Browell, E., Ferrare, R., and Blake, D.: Processes influencing ozone levels in Alaskan forest fire plumes during long-range transport over the North Atlantic, J. Geophys. Res.-Atmos., 112, D10S41, doi:10.1029/2006JD007576, 2007.

Reddy, M. S., Boucher, O., Balkanski, Y., and Schulz, M.: Aerosol optical depths and direct radiative perturbations by species and source type, Geophys. Res. Lett., 32, L12803, doi:10.1029/2004GL021743, 2005.

Roberts, G. C., Nenes, A., Seinfeld, J. H., and Andreae, M. O.: Impact of biomass burning on cloud properties in the Amazon Basin, J. Geophys. Res.-Atmos., 108(D2), 4062, doi:10.1029/2001JD000985, 2003.

Roeckner, E., Brasseur, G., Giorgetta, M., Jacob, D., Jungclaus, J., Reick, C., and Sillmann, J.: Climate projections for the 21st century, in: Internal Report, 28 p., Max Planck Institut für Meteorologie, available online: http://www.mpimet.mpg.de/fileadmin/grafik/presse/ClimateProjections2006.pdf, last access: December 2011, 2006.

Rogers, B. M., Neilson, R. P., Drapek, R., Lenihan, J. M., Wells, J. R., Bachelet, D., and Law, B. E.: Impacts of climate change on fire regimes and carbon stocks of the US Pacific Northwest, J. Geophys. Res.-Biogeo., 116, G03037, doi:10.1029/2011JG001695, 2011.

Sakaguchi, K. and Zeng, X.: Effects of soil wetness, plant litter, and under-canopy atmospheric stability on ground evaporation in the Community Land Model (CLM3.5), J. Geophys. Res., 114, D01107, doi:10.1029/2008JD010834, 2009.

Sakaeda, N., Wood, R., and Rasch, P. J.: Direct and semidirect aerosol effects of Southern African biomass burning aerosol, J. Geophys. Res.-Atmos., 116, D12205, doi:10.1029/2010JD015540, 2011.

ACPD
12, 10535–10621, 2012

Schwarz, J. P., Gao, R. S., Spackman, J. R., Watts, L. A., Thomson, D. S., Fahey, D. W., Ryerson, T. B., Peischl, J., Holloway, J. S., Trainer, M., Frost, G. J., Baynard, T., Lack, D. A., de Gouw, J. A., Warneke, C., and Del Negro, L. A.: Measurement of the mixing state, mass, and optical size of individual black carbon particles in urban and biomass burning emissions, Geophys. Res. Lett., 35, L13810, doi:10.1029/2008GL033968, 2008.

Seinfeld, J. H. and Pandis, S. N.: Atmospheric Chemistry and Physics: From Air Pollution to Climate Change, 2nd edn., Wiley-Interscience, New York, 2006.

Siegenthaler, U. and Joos, F.: Use of a simple model for studying oceanic tracer distributions and the global carbon cycle, Tellus, 44, 186–207, 1992.

Solomon, S., Qin, D., Manning, M., Chen, Z., Marquis, M., Averyt, K. B., Tignor, M., and Miller, H. L. (Eds.): Contribution of Working Group I to the Fourth Assessment Report of the Intergovernmental Panel on Climate Change, 996 pp., Cambridge University Press, Cambridge, UK and New York, NY, USA, 2007.

Stoeckli, R., Lawrence, D. M., Niu, G.-Y., Oleson, K. W., Thornton, P. E., Yang, Z.-L., Bonan, G. B., Denning, A. S., and Running, S. W.: The use of Fluxnet in the Community Land Model development, J. Geophys. Res., 113, G01025, doi:10.1029/2007JG000562, 2008.

Stohl, A., Berg, T., Burkhart, J. F., Fjaeraa, A. M., Forster, C., Herber, A., Hov, Ø., Lunder, C., McMillan, W. W., Oltmans, S., Shiobara, M., Simpson, D., Solberg, S., Stebel, K., Ström, J., Tørseth, K., Treffeisen, R., Virkkunen, K., and Yttri, K. E.: Arctic smoke – record high air pollution levels in the European Arctic due to agricultural fires in Eastern Europe in spring 2006, Atmos. Chem. Phys., 7, 511–534, doi:10.5194/acp-7-511-2007, 2007.

Stone, R. S., Augustine, J. A., Dutton, E. G., O'Neill, N. T., and Saha, A.: Empirical determinations of the longwave and shortwave radiative forcing efficiencies of wildfire smoke, J. Geophys. Res.-Atmos., 116, D12207, doi:10.1029/2010JD015471, 2011.

Syakila, A. and Kroeze, C.: The global nitrous oxide budget revisited, Greenhouse Gas Meas. Manag., 1, 17–26, doi:10.3763/ghgmm.2010.0007, 2011.

Thonicke, K., Venevsky, S., Sitch, S., and Cramer, W.: The role of fire disturbance for global vegetation dynamics: coupling fire into a Dynamic Global Vegetation Model, Global Ecol. Biogeogr., 10, 661–678, 2001.

Thonicke, K., Spessa, A., Prentice, I. C., Harrison, S. P., Dong, L., and Carmona-Moreno, C.: The influence of vegetation, fire spread and fire behaviour on biomass burning and trace gas emissions: results from a process-based model, Biogeosciences, 7, 1991–2011, doi:10.5194/bg-7-1991-2010, 2010.

ACPD
12, 10535–10621, 2012

Thornton, P. E., Lamarque, J. F., Rosenbloom, N. A., and Mahowald, N. M.: Influence of carbon-nitrogen cycle coupling on land model response to CO_2 fertilization and climate variability, Global Biogeochem. Cy., 21, GB4018, doi:1029/2006GB002868, 2007.

Thornton, P. E., Doney, S. C., Lindsay, K., Moore, J. K., Mahowald, N., Randerson, J. T., Fung, I., Lamarque, J.-F., Feddema, J. J., and Lee, Y.-H.: Carbon-nitrogen interactions regulate climate-carbon cycle feedbacks: results from an atmosphere-ocean general circulation model, Biogeosciences, 6, 2099–2120, doi:10.5194/bg-6-2099-2009, 2009.

Tosca, M. G., Randerson, J. T., Zender, C. S., Flanner, M. G., and Rasch, P. J.: Do biomass burning aerosols intensify drought in equatorial Asia during El Niño?, Atmos. Chem. Phys., 10, 3515–3528, doi:10.5194/acp-10-3515-2010, 2010.

Tosca, M. G., Randerson, J. T., Zender, C. S., Nelson, D. L., Diner, D. J., and Logan, J. A.: Dynamics of fire plumes and smoke clouds associated with peat and deforestation fires in Indonesia, J. Geophys. Res.-Atmos, 116, D08207, doi:10.1029/2010JD015148, 2011.

Val Martin, M., Logan, J. A., Kahn, R. A., Leung, F.-Y., Nelson, D. L., and Diner, D. J.: Smoke injection heights from fires in North America: analysis of 5 years of satellite observations, Atmos. Chem. Phys., 10, 1491–1510, doi:10.5194/acp-10-1491-2010, 2010.

Veraverbeke, S., Lhermitte, S., Verstraeten, W. W., and Goossens, R.: A time-integrated MODIS burn severity assessment using the multi-temporal differenced normalized burn ratio ($dNBR_{MT}$), Int. J. Appl. Earth Obs., 13, 52–58, doi:10.1016/j.jag.2010.06.006, 2011.

Vitousek, P.: Litterfall, nutrient cycling and nutrient limitations in tropical forests, Ecology, 65, 285–298, 1984.

Wang, A. H. and Zeng, X. B.: Improving the treatment of the vertical snow burial fraction over short vegetation in the NCAR CLM3, Adv. Atmos. Sci., 26, 5, doi:10.1007/s00376-009-80983, 2009.

Wang, M., Ghan, S., Ovchinnikov, M., Liu, X., Easter, R., Kassianov, E., Qian, Y., and Morrison, H.: Aerosol indirect effects in a multi-scale aerosol-climate model PNNL-MMF, Atmos. Chem. Phys., 11, 5431–5455, doi:10.5194/acp-11-5431-2011, 2011.

Wang, Q., Jacob, D. J., Fisher, J. A., Mao, J., Leibensperger, E. M., Carouge, C. C., le Sager, P., Kondo, Y., Jimenez, J. L., Cubison, M. J., and Doherty, S. J.: Sources of carbonaceous aerosols and deposited black carbon in the Arctic in winter-spring: implications for radiative forcing, Atmos. Chem. Phys. Discuss., 11, 19395–19442, doi:10.5194/acpd-11-19395-2011, 2011.

ACPD
12, 10535–10621, 2012

van der Werf, G. R., Randerson, J. T., Giglio, L., Collatz, G. J., Kasibhatla, P. S., and Arellano Jr., A. F.: Interannual variability in global biomass burning emissions from 1997 to 2004, Atmos. Chem. Phys., 6, 3423–3441, doi:10.5194/acp-6-3423-2006, 2006.

van der Werf, G. R., Dempewolf, J., Trigg, S. N., Randerson, J. T., Giglio, L., Murdiyarso, D., Peters, W., Morton, D. C., Collatz, G. J., Dolman, A. J., and DeFries, R. S.: Climate regulation of fire emissions and deforestation in equatorial Asia, Proc. Natl. Acad. Sci., 105, 20350–20355, doi:10.1073/pnas.0803375105, 2008.

van der Werf, G. R., Randerson, J. T., Giglio, L., Collatz, G. J., Mu, M., Kasibhatla, P. S., Morton, D. C., DeFries, R. S., Jin, Y., and van Leeuwen, T. T.: Global fire emissions and the contribution of deforestation, savanna, forest, agricultural, and peat fires (1997–2009), Atmos. Chem. Phys., 10, 11707–11735, doi:10.5194/acp-10-11707-2010, 2010.

White, C. S. and Loftin, S. R.: Response of 2 semiarid grasslands to cool-season prescribed fire, J. Range Manage., 53, 52–61, doi:10.2307/4003392, 2000.

Wilcox, E. M.: Stratocumulus cloud thickening beneath layers of absorbing smoke aerosol, Atmos. Chem. Phys., 10, 11769–11777, doi:10.5194/acp-10-11769-2010, 2010.

Wild, O. and Prather, M. J.: Excitation of the primary tropospheric chemical mode in a global 3-D model, J. Geophys. Res., 105, 24647–24660, 2000.

Zhang, L., Li, Q. B., Jin, J., Liu, H., Livesey, N., Jiang, J. H., Mao, Y., Chen, D., Luo, M., and Chen, Y.: Impacts of 2006 Indonesian fires and dynamics on tropical upper tropospheric carbon monoxide and ozone, Atmos. Chem. Phys., 11, 10929–10946, doi:10.5194/acp-11-10929-2011, 2011.

ACPD
12, 10535–10621, 2012

Table 1. A list of the simulations used in this study with details given about the model configuration and emissions used. The run length specifies the number of years simulated with year 2000 climate, or, where a range is specified, exact time periods.

Class	Model Configuration	Simulation	Fire Emissions	Background Emissions	Run length (yr)
CHEM	CAM4.9 standalone	CHEM_1850_NF	-	1850	1
	– MOZART tropospheric chemistry	CHEM_1850_KF	CLM	1850	1
	– Data ocean model	CHEM_2000_NF	–	2000	1
	– Year 2000 climate	CHEM_2000_KF	CLM	2000	1
	– Prescribed aerosol,	CHEM_2000_GF	GFED	2000	1
	ghg forcing	CHEM_2100_NF	–	2100-RCP45	1
		CHEM_2100_CKF	CLM-CCSM	2100-RCP45	1
		CHEM_2100_EKF	CLM-ECHAM	2100-RCP45	1
AERO	CAM5 standalone	AERO_1850_NF	–	1850	5
	– Modal Aerosol Model	AERO_1850_KF	CLM	1850	5
	– Data ocean model	AERO_2000_NF	–	2000	5
	– Year 2000 climate	AERO_2000_KF	CLM	2000	5
	– Radiatively-active	AERO_2000_GF	GFED	2000	5
	aerosols	AERO_2100_NF	–	2100-RCP45	5
		AERO_2100_CKF	CLM-CCSM	2100-RCP45	5
		AERO_2100_EKF	CLM-ECHAM	2100-RCP45	5
CO_2	CLM3.5 with CN	CO2_NF_past	–	–	1798–2000
	– ATM forcing: CCSM	CO2_NF_ftr_CCSM	–	–	2000–2100
	or ECHAM	CO2_NF_ftr_ECHAM	–	–	2000–2100
	– NF = No fire activity	CO2_KF_past	–	–	1798–2000
	– KF = Kloster et al. (2010)	CO2_KF_ftr_CCSM	–	–	2000–2100
	fires active	CO2_KF_ftr_ECHAM	–	–	2000–2100

ACPD
12, 10535–10621, 2012

Table 2. Global annual average chemical quantities for all simulations in the CHEM group. RFs are given in $W m^{-2}$ and the CH_4 lifetime is given in yr. Percentage values show the proportional change relative to the no-fire (NF) quantity for the given time period.

Simulation	$[O_3]$		O_3 RF		[OH]	CH_4	
	sfc (ppb)	sfc – chem. trop. (DU)	Short-lived	Primary mode	sfc – 200 mb (10^6 molec. cm^{-3})	$\tau(CH_4)$	RF
CHEM_1850_NF	10	12	–	–	0.6	14	–
CHEM_1850_KF	+18%	+15%	0.07	−0.03	+18%	11.4	−0.05
CHEM_2000_NF	26	27	–	–	1.0	8.8	–
CHEM_2000_KF	+2%	+2%	0.02	0.01	−4%	9.1	0.05
CHEM_2000_GF	+1%	0%	0	0.03	−11%	9.7	0.13
CHEM_2100_NF	23	25	–	–	1.0	8.4	–
CHEM_2100_CKF	+3%	+2%	0.02	0.02	−6%	8.8	0.08
CHEM_2100_EKF	+4%	+3%	0.03	0.03	−10%	9	0.13

ACPD
12, 10535–10621, 2012

Table 3. Values used for the N_2O box model equilibrium runs and the results of these runs. The atmospheric forcing used for future fire emissions is given in parentheses in the "case" column, C for CCSM and E for ECHAM forcing.

Case	Initial $[N_2O]$ [a] ppbv	Emissions from fire [b] $TgN\,yr^{-1}$	Total Emissions [c] $TgN\,yr^{-1}$	Equilibrium $[N_2O]$ [d] ppbv	$[N_2O]$ from fire emis. ppbv	N_2O from fire emis. RF $W\,m^{-2}$
1850 – All emis.	275	–	11.7	279	–	–
1850 – No CLM3 fire emis.	275	0.45	11.2	269	10	0.03
2000 – All emis.	316	–	15.7	369	–	–
2000 – No CLM3 fire emis.	316	0.40	15.3	360	9	0.03
2000 – No GFED fire emis.	316	0.58	15.1	356	13	0.04
2100 – All emis.	372	–	17.1	401	–	–
2100 – No CLM3(C) fire emis.	372	0.50	16.6	390	11	0.03
2100 – No CLM3(E) fire emis.	372	0.72	16.4	385	16	0.04

[a] Initial $[N_2O]$ values are taken from the RCP4.5 emission time series of Meinshausen et al. (2011a).

[b] Fire emissions are global averages computed from the CLM3 simulations.

[c] Total emissions (minus fire emissions where applicable) are the sum of anthropogenic emissions of N_2O from Meinshausen et al. (2011a) and natural emissions computed using Eq. (A28) from Meinshausen et al. (2011a), with allowances for the transport time of emitted N_2O to the stratosphere and lifetime feedback, given by Meinshausen et al. (2011b).

[d] Lifetime is recalculated every model year for the new N_2O concentration when running to equilibrium.

ACPD
12, 10535–10621, 2012

Table 4. Global annual average forcing terms for aerosols in all CAM5 simulations. All figures are given in $W m^{-2}$, except for the global, annual total BC and OC emissions. The indirect effects are equivalent to the change in LWCF added to the change in SWCF.

Simulation	BC + OC Emission [$Tg yr^{-1}$]	TOA SW Aerosol forcing	Direct effect		Cloud forcing		Indirect effects
			Clr-sky	All-sky	LW	SW	
AERO_1850_NF	5.7	−1.42	–	–	24.0	−49.7	–
AERO_1850_KF	84	−1.32	−0.15	0.10	23.7	−51.0	−1.60
AERO_2000_NF	18	−1.51	–	–	24.4	−52.5	–
AERO_2000_KF	90	−1.41	−0.15	0.10	24.1	−53.2	−1.00
AERO_2000_GF	150	−1.38	−0.27	0.13	24.0	−53.7	−1.64
AERO_2100_NF	5.8	−1.46	–	–	24.1	−50.6	–
AERO_2100_CKF	98	−1.34	−0.24	0.12	23.8	−51.6	−1.42
AERO_2100_EKF	140	−1.21	−0.25	0.25	23.5	−51.7	−1.74

ACPD
12, 10535–10621, 2012

Table 5. Radiative forcings for all fire impacts considered in this study. All values are given in $W m^{-2}$. The direct effect for clear sky values are not included in the total.

FORCING	1850	2000		2100		EFFICACY [a]
	CLM3	CLM3 fire	GFEDv2	CLM3-fire CCSM	CLM3-fire ECHAM	
Tropospheric Ozone	0.04	0.03	0.03	0.04	0.06	0.82
Methane	−0.05	0.05	0.13	0.08	0.13	1.45
Nitrous Oxide	0.03	0.03	0.04	0.03	0.04	1.04
Carbon Dioxide	0.83	0.62	–	0.75	0.91	1
Direct Effect – All sky	0.10	0.10	0.13	0.12	0.25	0.58, 0.91 [b]
Direct Effect – Clr sky	−0.15	−0.15	−0.27	−0.24	−0.25	–
Indirect Cloud Effects	−1.60	−1.00	−1.64	−1.42	−1.74	–
Indirect BGC Effects	−0.09 ± 0.09	−0.08 ± 0.08	−0.15 ± 0.12	−0.10 ± 0.09	−0.13 ± 0.10	–
Land Albedo Changes	−0.19	−0.18	−0.10	−0.21	−0.26	–
Snow Albedo Changes	0.00	0.00	0.01	0.00	0.00	1.7
Feedback onto C-cycle	−0.26 ± 0.26	−0.09 ± 0.09	–	−0.09 ± 0.09	−0.10 ± 0.10	–
TOTAL	−1.19	−0.52	–	−0.80	−0.84	–

[a] Efficacy values were taken from Hansen et al. (2005).

[b] Efficacy for direct effects of black carbon and organic carbon aerosols from fires, respectively.

ACPD
12, 10535–10621, 2012

Table A1. Regression of the monthly mean model and satellite aerosol parameters onto the AERONET observations for all months and all AERONET stations. Coefficients are the slope of the linear regression, the *y*-intercept, the correlation coefficient, the root mean squared error, the slope when forced through point (0,0), and the adjustment factor for the satellite AOD. Italics represent the results of computations on the subset of observations for which the satellite AOD > 0.2.

	SLOPE	INTERCEPT	R^2	RMSE	ZI-SLOPE	AOD-adj
CAM AOD	0.34	0.07	0.29	0.10		
MODIS AOD	*0.45*	*0.18*	*0.51*	*0.10*	*0.81*	*1.23*
MISR AOD	*0.23*	*0.20*	*0.43*	*0.06*	*0.58*	*1.72*
CAM SSA	0.57	0.36	0.33	0.03		
MISR SSA	*0.23*	*0.76*	*0.06*	*0.03*		
CAM AAOD [a]	0.17	0.03	0.03	0.02		
MISR AAOD	*0.06*	*0.01*	*0.08*	*0.01*		

[a] AAOD equals the absorbing AOD, or the portion of the AOD that is not due to scattering.

ACPD
12, 10535–10621, 2012

Table A2. Values of the scaling factors α and β for the seven GFED regions with annual fire emissions of greater than 100 TgC yr^{-1}. The values of α for MODIS and MISR data were averaged and rounded to the nearest multiple of 0.5 to give the scaling factor used in the forward model simulations.

	MODIS		MISR		Scaling
Region	β	α	β	α	Factor
SHSA	1.61	1.87	2.43	1.82	2.0
NHAF	0.89	0.48	0.79	1.09	1.0
SHAF	2.13	2.59	2.33	3.52	3.0
BOAS	1.11	3.88	4.39	2.13	3.0
SEAS	2.53	1.37	2.48	1.81	1.5
EQAS	3.63	2.51	3.67	3.32	3.0
AUST	1.15	1.40	1.43	3.47	2.5

ACPD
12, 10535–10621, 2012

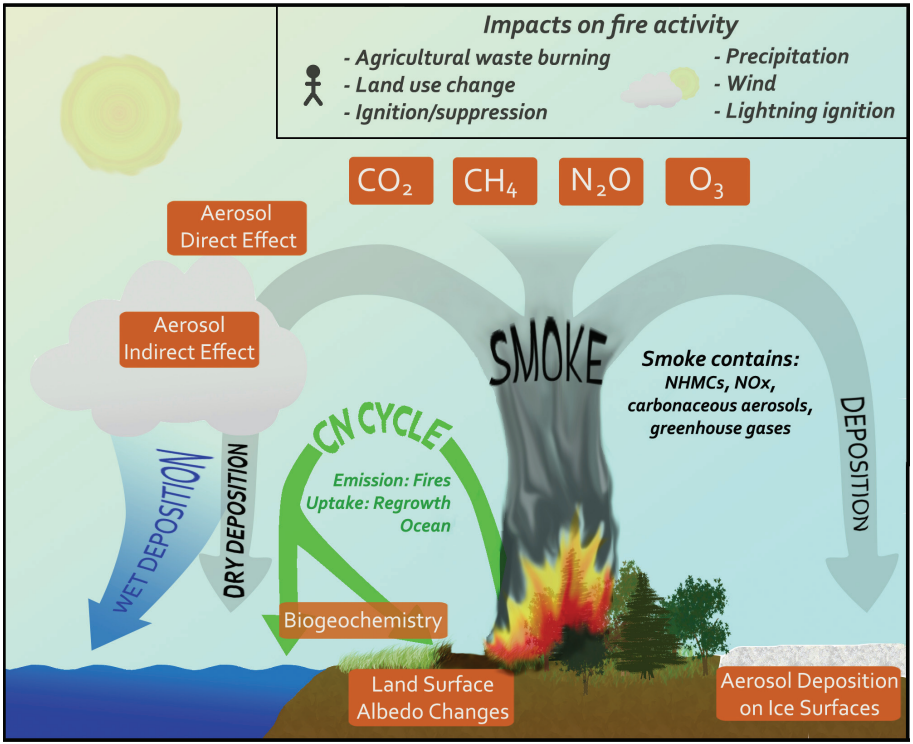

Fig. 1. A schematic illustrating the various impacts of fire on the atmosphere, land surface, ice surfaces and the ocean.

ACPD
12, 10535–10621, 2012

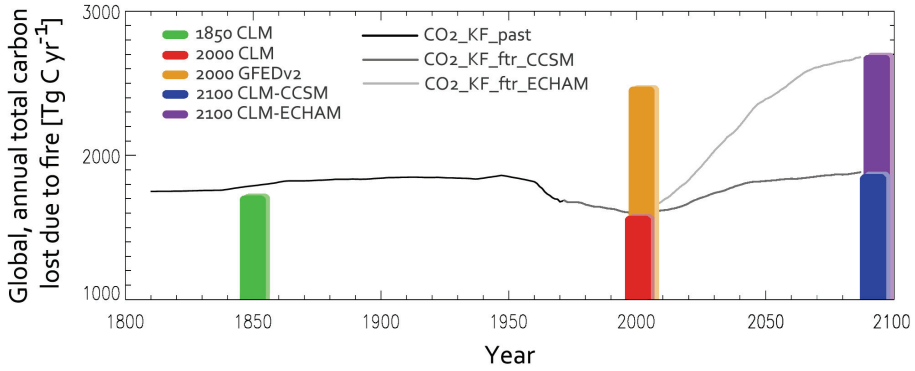

Fig. 2. Timeseries of the total C lost due to fires predicted by CLM3 (Kloster et al., 2012). The timeseries is smoothed using a 25-yr running average. Ten-year average values used to compute fire emissions for each time period are highlighted in color.

ACPD
12, 10535–10621, 2012

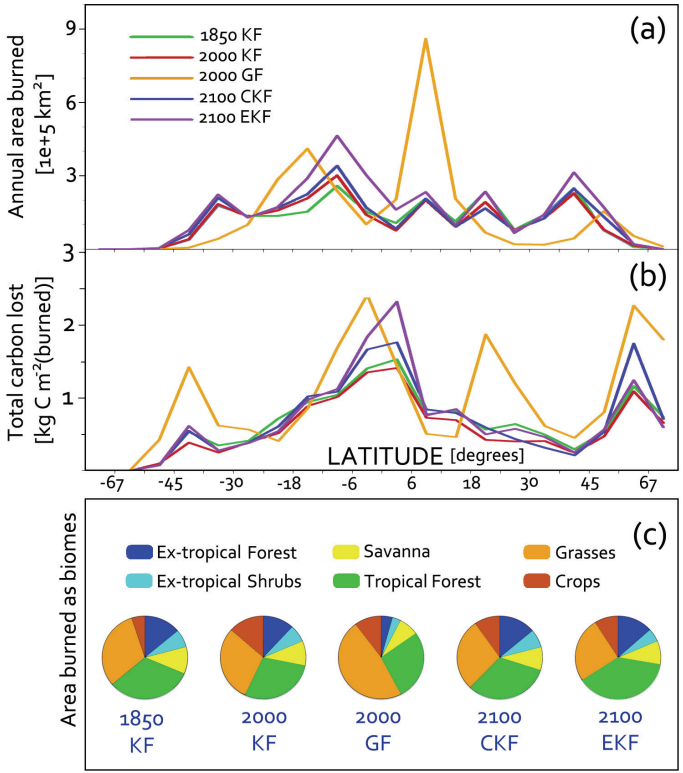

Fig. 3. A plot by latitude of **(a)** the annual total area burned for each 10-yr emissions period and **(b)** the amount of C released per area burned, and **(c)** a breakdown of the global annual average area burned into biomes defined by the CLM3 PFTs database for the respective time periods. Note that the latitude bands each contain approximately the same surface area for better comparison of the total area burned across latitudes.

ACPD
12, 10535–10621, 2012

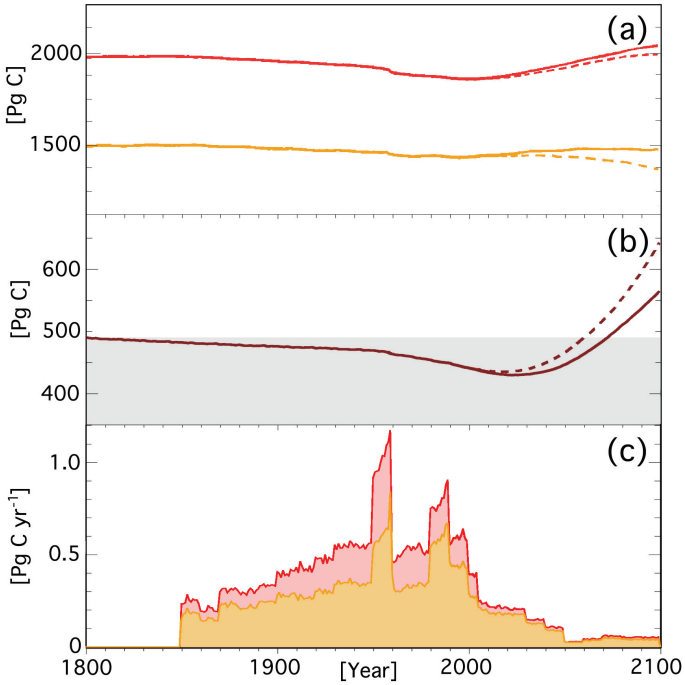

Fig. 4. Timeseries of **(a)** the total C stored in terrestrial ecosystems, **(b)** difference in total C stored in terrestrial ecosystems between the CO2_NF and CO2_KF simulation sets, and **(c)** total C lost due to land-use changes, plotted for the CO2_NF simulations (red; panels **(a)** and **(c)** and the CO2_KF simulations (orange; panels **(a)** and **(c)**). Timeseries are plotted for the simulations with the CCSM (solid lines) and ECHAM (dashed lines) future atmospheric forcing. The shaded region in **(b)** indicates when the change in carbon storage due to removing fires is less than the initial (1798), preindustrial value.

ACPD
12, 10535–10621, 2012

The changing radiative forcing of fires

D. S. Ward et al.

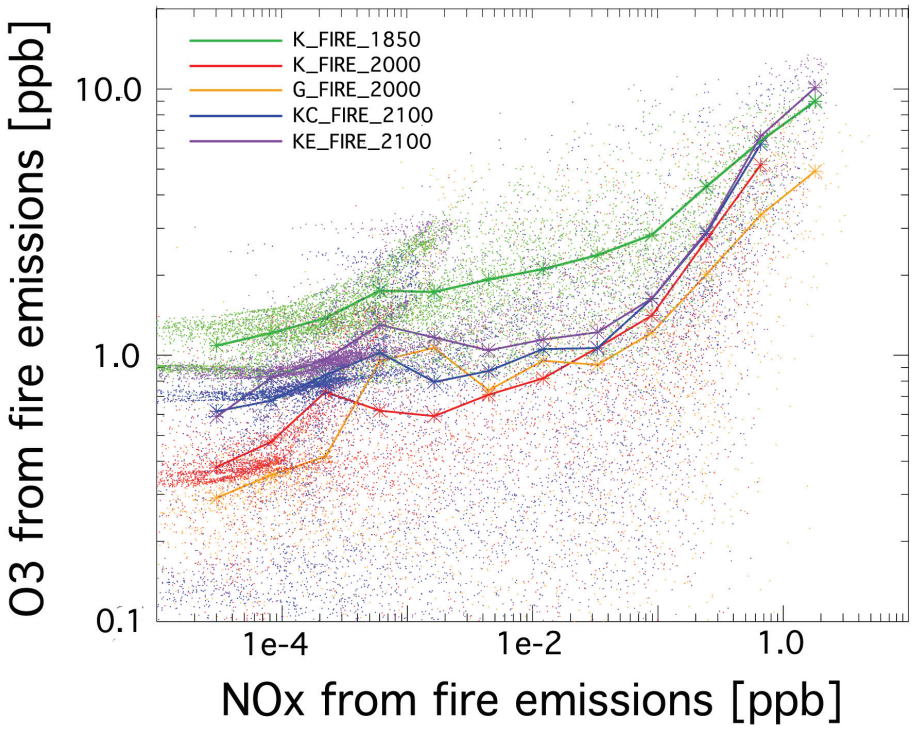

Fig. 5. Scatterplot of annual average NO_x produced from fire emissions against O_3 produced from fire emissions for surface level grid points with non-zero fire emissions. The points were binned by values of NO_x produced and averaged, shown as the solid lines. Both axes are plotted on logarithmic scales for ease of view.

ACPD
12, 10535–10621, 2012

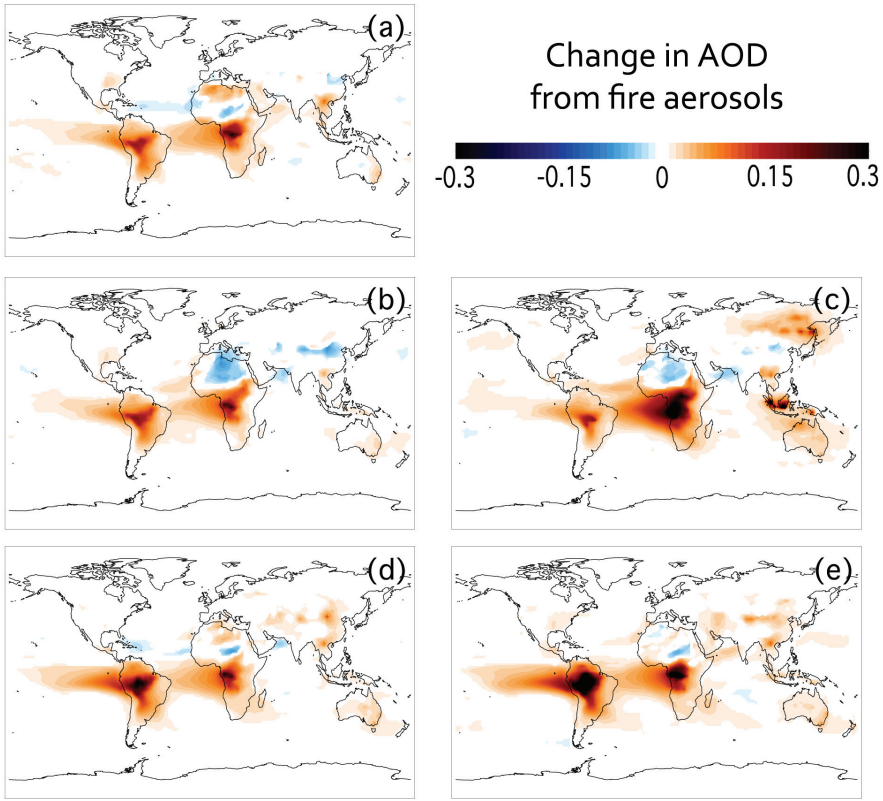

Fig. 6. The annual average change in AOD from fire aerosols for **(a)** 1850-KF, **(b)** 2000-KF, **(c)** 2000-GF, **(d)** 2100-CKF, and **(e)** 2100-EKF.

ACPD
12, 10535–10621, 2012

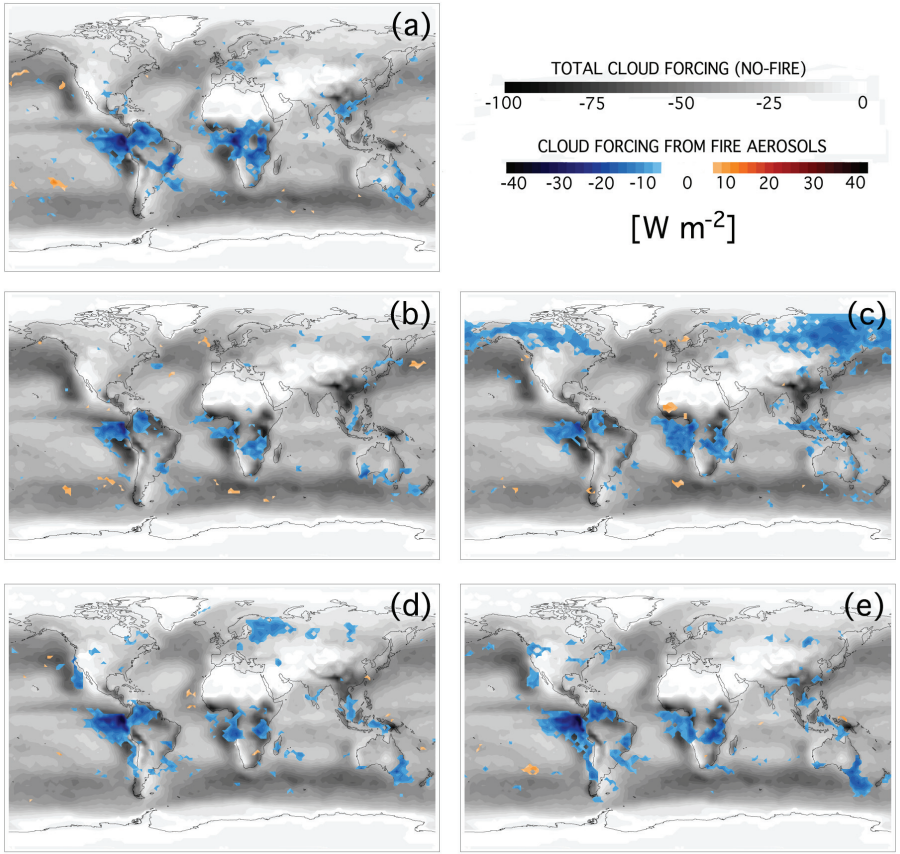

Fig. 7. The annual average change in total cloud forcing from fire aerosols plotted in color for **(a)** 1850-KF, **(b)** 2000-KF, **(c)** 2000-GF, **(d)** 2100-CKF, and **(e)** 2100-EKF. The grey-scale shading shows the annual average total cloud forcing in the no-fire simulation corresponding to the plotted emissions year.

ACPD
12, 10535–10621, 2012

The changing radiative forcing of fires

D. S. Ward et al.

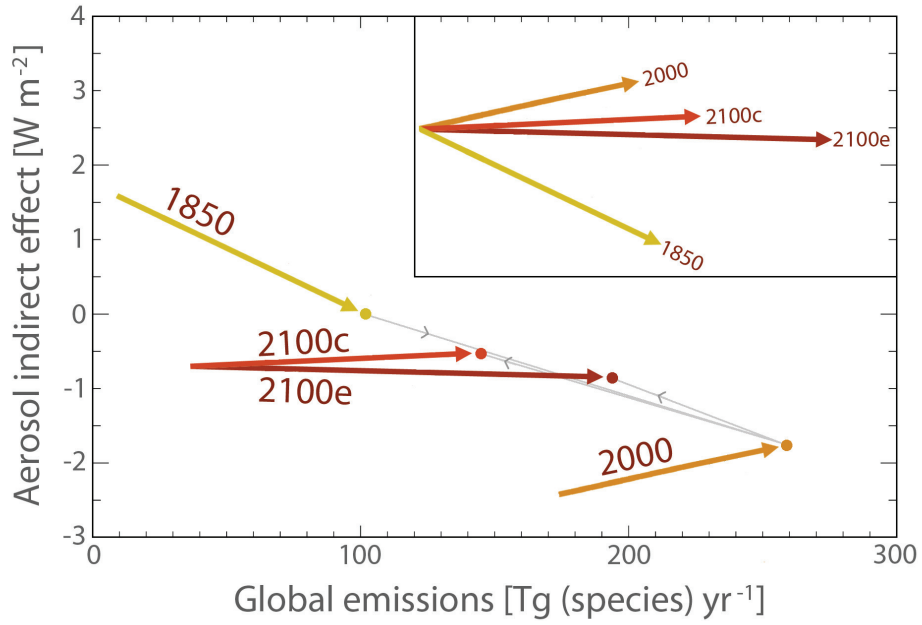

Fig. 8. Global annual average emissions of BC, OC and SO_2 (assumed to convert to SO_4) plotted against the aerosol indirect effects computed from CAM5 for all time periods and both future atmospheric forcings, represented as colored circles. The arrows trace the change due to fire aerosols. The change in indirect effects are references against a preindustrial value of $0\,W\,m^{-2}$. The top, right-hand panel highlights the change in angle between the fire impacts in the different time periods.

ACPD
12, 10535–10621, 2012

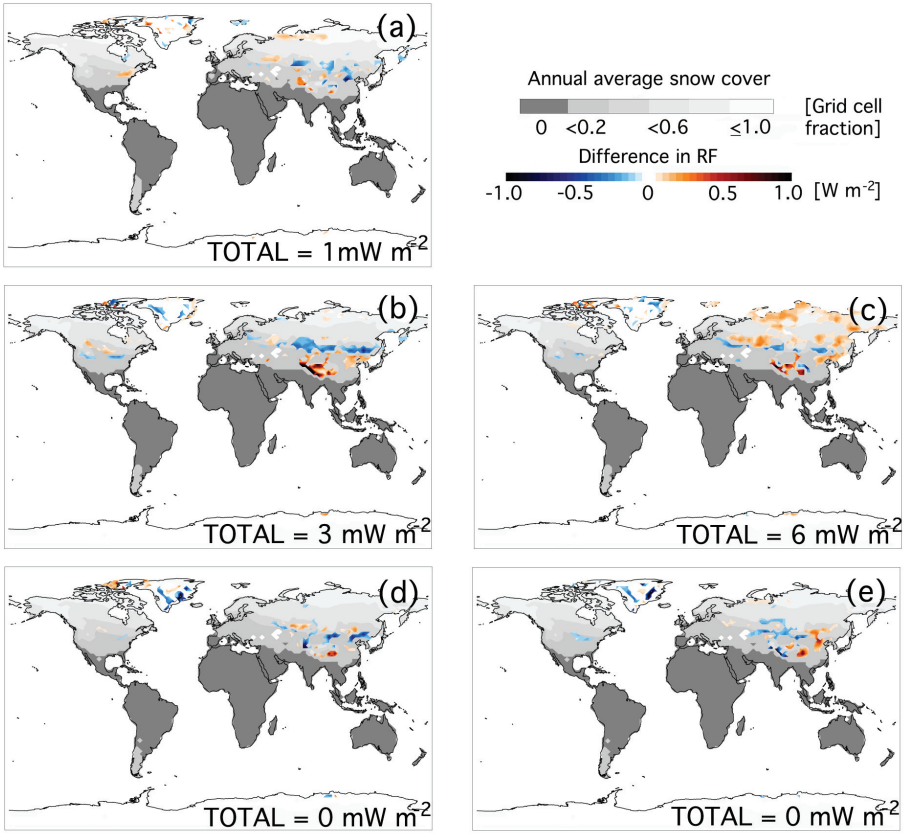

Fig. 9. The annual average difference in snow surface RF due to the deposition of fire aerosols for **(a)** 1850-KF, **(b)** 2000-KF, **(c)** 2000-GF, **(d)** 2100-CKF, and **(e)** 2100-EKF. This is plotted over the annual average snow cover (grey-scale) from the emissions-year corresponding no-fire simulation. The global, annual average is given at the bottom of each plot.

ACPD
12, 10535–10621, 2012

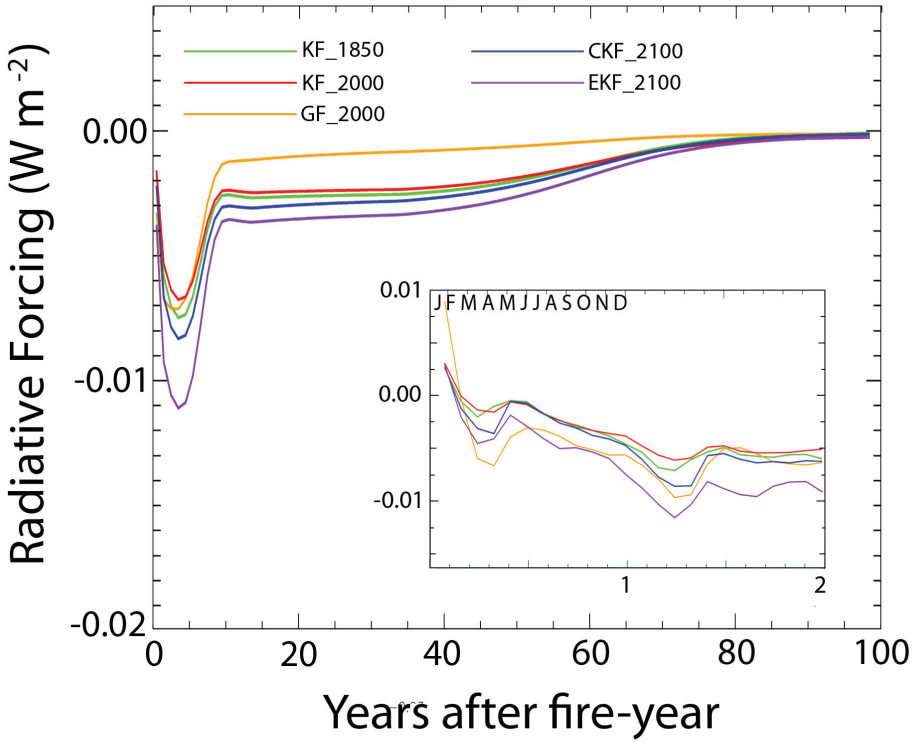

Fig. 10. A plot of the RF due to land surface albedo changes caused by fires and how it changes during the years following the fire disturbance. The main plot shows annual averaged RF beginning the year after a full year of fire activity. The detail plot breaks the RF down by month showing the annual cycle following one full year of fire activity. Fire emissions from CLM3 are marked as "KF" with "C" (CCSM) or "E" (ECHAM) future climate, and GFEDv2 emissions are marked as "GF".

ACPD
12, 10535–10621, 2012

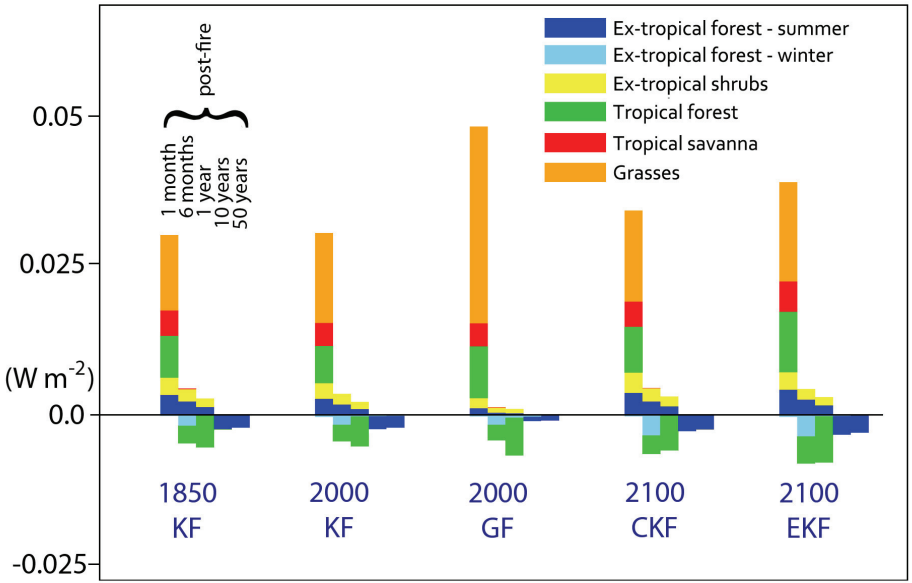

Fig. 11. A breakdown of the RF due to land surface albedo change from fires into major biomes and for different lengths of time after the fire occurred. Fire emissions are labeled as in Fig. 10.

ACPD
12, 10535–10621, 2012

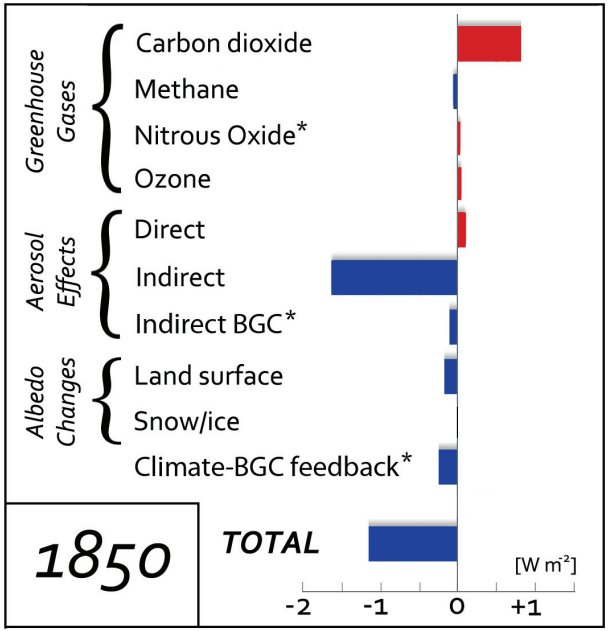

Fig. 12. Global, annual average RF for the various impacts of fires examined in this study, plotted for the preindustrial case. Asterisks indicate RFs that were computed using emissions data and not the CAM model integrations, or the CLM no-fire simulation used for the CO_2 RF.

ACPD
12, 10535–10621, 2012

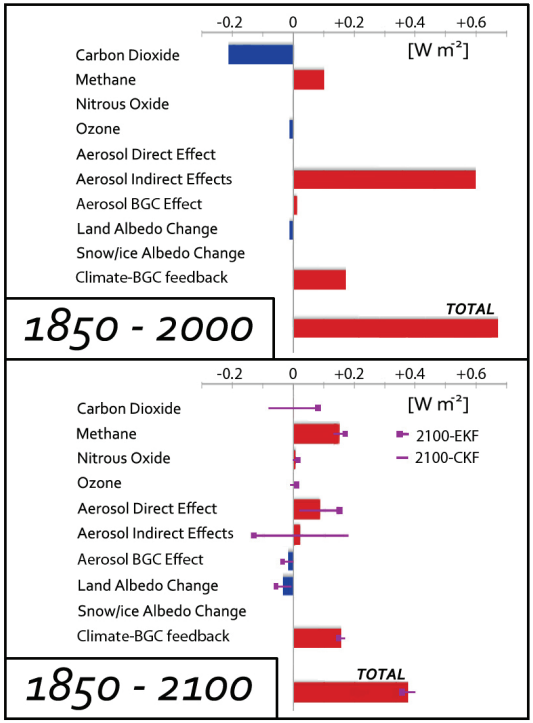

Fig. 13. Difference in the global, annual average RF for the various impacts of fire examined in this study between preindustrial and present day emissions (1850–2000) and through to the year 2100 (1850–2100). For 1850–2100, the average RF for the two sets of fire emissions used in 2100 is given with the range shown as the purple lines.

ACPD
12, 10535–10621, 2012

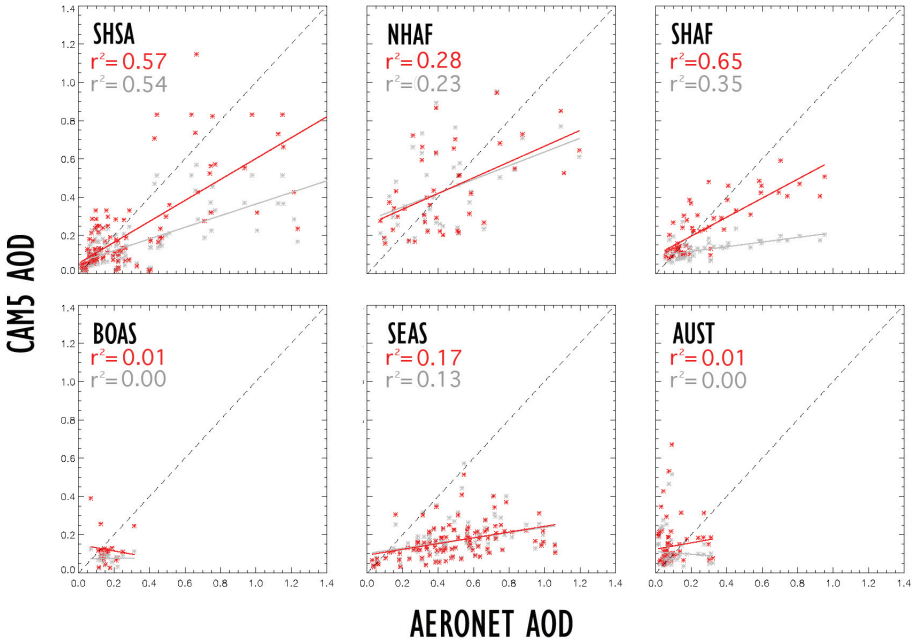

Fig. A1. Scatterplots of the monthly mean model AOD vs. AERONET AOD for different GFED regions and the globe. Results from simulations with both the un-scaled GFEDv2 emissions (gray) and scaled emissions (red) are shown. EQAS is excluded due to the small number of AERONET data points within this region. Linear regression lines are plotted.

ACPD
12, 10535–10621, 2012

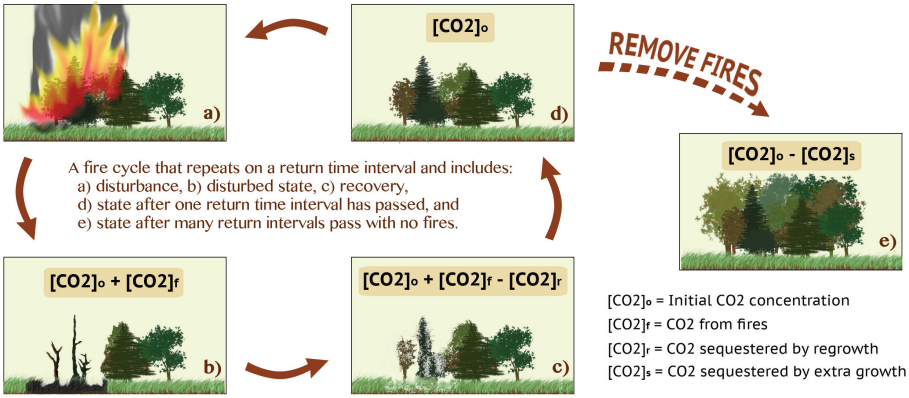

Fig. B1. A schematic representation of a fire cycle with associated CO_2 changes, and a simple illustration of the same ecosystem with fires removed.

ACPD
12, 10535–10621, 2012

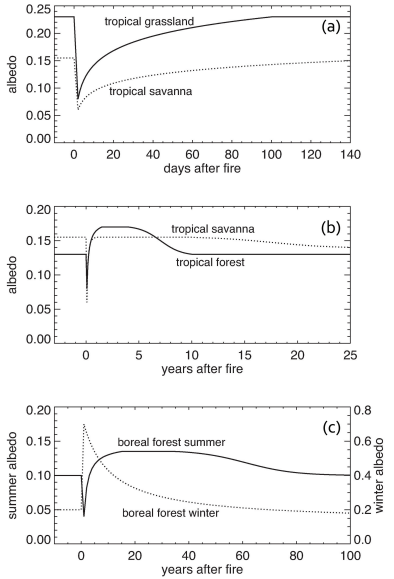

Fig. B2. Timeseries of surface albedo, estimated from past research, showing the recovery of different biomes from fire disturbance. Note the different timescales for panels **(a)** and **(b)** and the difference *y*-axis values for the winter and summer fires in panel **(c)**. These estimates were compiled from the following literature for tropical grasslands [1], tropical savanna[2], tropical forests[3], and boreal forests[4].

[1]Fisch et al. (1994), Fuller and Ottke (2002), Jin and Roy (2005), White and Loftin (2000)

[2]Beringer et al. (2003), Brookan-Amissah et al. (1980), Govaerts et al. (2002), Higgins et al. (2007), Jin and Roy (2005), Myhre et al. (2005)

[3]Culf et al. (1995), Giambelluca et al. (1997), Pinker et al. (1980)

[4]Amiro et al. (2006), Lyons et al. (2008), McMillan et al. (2008)

ACPD
12, 10535–10621, 2012